

Article

Structural optimization of 4-chlorobenzoylpiperidine derivatives for the development of potent, reversible and selective monoacylglycerol lipase (MAGL) inhibitors

Carlotta Granchi, Flavio Rizzolio, Stefano Palazzolo, Sara Carmignani, Marco Macchia, Giuseppe Saccomanni, Clementina Manera, Adriano Martinelli, Filippo Minutolo, and Tiziano Tuccinardi

J. Med. Chem., **Just Accepted Manuscript** • DOI: 10.1021/acs.jmedchem.6b01459 • Publication Date (Web): 03 Nov 2016

Downloaded from <http://pubs.acs.org> on November 7, 2016

Just Accepted

“Just Accepted” manuscripts have been peer-reviewed and accepted for publication. They are posted online prior to technical editing, formatting for publication and author proofing. The American Chemical Society provides “Just Accepted” as a free service to the research community to expedite the dissemination of scientific material as soon as possible after acceptance. “Just Accepted” manuscripts appear in full in PDF format accompanied by an HTML abstract. “Just Accepted” manuscripts have been fully peer reviewed, but should not be considered the official version of record. They are accessible to all readers and citable by the Digital Object Identifier (DOI®). “Just Accepted” is an optional service offered to authors. Therefore, the “Just Accepted” Web site may not include all articles that will be published in the journal. After a manuscript is technically edited and formatted, it will be removed from the “Just Accepted” Web site and published as an ASAP article. Note that technical editing may introduce minor changes to the manuscript text and/or graphics which could affect content, and all legal disclaimers and ethical guidelines that apply to the journal pertain. ACS cannot be held responsible for errors or consequences arising from the use of information contained in these “Just Accepted” manuscripts.

1
2
3
4
5
6
7
8
9
10
11
12
13
14
15
16
17
18
19
20
21
22
23
24
25
26
27
28
29
30
31
32
33
34
35
36
37
38
39
40
41
42
43
44
45
46
47
48
49
50
51
52
53
54
55
56
57
58
59
60

Structural optimization of 4-chlorobenzoylpiperidine derivatives for the development of potent, reversible and selective monoacylglycerol lipase (MAGL) inhibitors

Carlotta Granchi,[†] Flavio Rizzolio,^ϕ Stefano Palazzolo,^{ϕ,§} Sara Carmignani,[†] Marco Macchia,[†] Giuseppe Saccomanni,[†] Clementina Manera,[†] Adriano Martinelli,[†] Filippo Minutolo,[†] Tiziano Tuccinardi[†]*

[†] Department of Pharmacy, University of Pisa, Via Bonanno 6, 56126 Pisa, Italy

^ϕ Division of Experimental and Clinical Pharmacology, Department of Molecular Biology and Translational Research, National Cancer Institute and Center for Molecular Biomedicine, IRCCS, 33081 Aviano (PN), Italy

[§] Graduate School in Nanotechnology, University of Trieste, Trieste, Italy

ABSTRACT

Monoacylglycerol lipase (MAGL) inhibitors are considered potential therapeutic agents for a variety of pathological conditions, including several types of cancer. Many MAGL inhibitors are reported in literature; however, most of them showed an irreversible mechanism of action, which caused important side effects. The use of reversible MAGL inhibitors has been only partially investigated so far, mainly because of the lack of compounds with good MAGL reversible inhibition properties. In this study, starting from the (4-(4-chlorobenzoyl)piperidin-1-yl)(4-methoxyphenyl)methanone (CL6a) lead compound that showed a reversible mechanism of MAGL inhibition ($K_i = 8.6 \mu\text{M}$), we started its structural optimization and we developed a new potent and selective MAGL inhibitor (**17b**, $K_i = 0.65 \mu\text{M}$). Furthermore, modeling studies suggested that the binding interactions of this compound replace a structural water molecule reproducing its H-bonds in the MAGL binding site, thus identifying a new key anchoring point for the development of new MAGL inhibitors.

INTRODUCTION

Among the different endogenous lipids with endocannabinoid-like activity, anandamide (AEA) and 2-arachidonoylglycerol (2-AG) are the two most important endogenous ligands that are able to activate the G protein-coupled cannabinoid receptors, CB₁ and CB₂.¹ These endocannabinoids are produced on demand through stimulus-dependent cleavage of phospholipid precursors and they modulate multiple physiological processes including pain, inflammation, appetite, memory, and emotion and their signaling functions terminate by enzymatic hydrolysis.^{2,3} In the nervous system, 2-AG is produced by phospholipase C and diacylglycerol lipase and it is deactivated through hydrolysis mediated by monoacylglycerol lipase (MAGL). Because of the prominent role in 2-AG degradation, selective inactivation of MAGL represents a potential target for pharmacological

agents able to treat diverse pathological conditions such as cancer, chronic pain and Alzheimer's disease.⁴ In the past ten years, massive efforts have been implemented in order to obtain potent MAGL inhibitors,⁵⁻¹⁰ however, almost all the compounds found showed irreversible inhibition properties.¹¹ In this context the reference inhibitors that have been used in the literature for most cellular and animal experiments are 4-nitrophenyl-4-[bis(1,3-benzodioxol-5-yl)(hydroxy)methyl]piperidine-1-carboxylate **1** (JZL184, Figure 1)⁸ and the benzyl(4-(5-methoxy-2-oxo-1,3,4-oxadiazol-3(2*H*)-yl)-2-methylphenyl)carbamate **2** (CAY10499, Figure 1).⁵ As reported by Scholsburg and co-workers, the irreversible inhibition of MAGL, induced by repeated administration of **1**, yielded cross-tolerance to CB₁ agonists in mice.¹² Chronic MAGL inhibition also produced physical dependence, desensitized brain CB₁ receptors and damaged endocannabinoid-dependent synaptic plasticity.¹² Genetic inactivation of MAGL or prolonged pharmacological blockage of MAGL by an irreversible inhibitor provokes the persistence of elevated 2-AG levels in the brain. This fact leads to a tolerance of the effects induced by MAGL inhibition. Moreover, responses to CB₁ agonists were significantly reduced and there was an evident cross-tolerance when exogenous CB₁ agonists were administered, resulting in a general CB₁ desensitization. Furthermore, profound alterations to CB₁ receptor expression and function in the brain were observed. Considering all these drawbacks associated to an irreversible MAGL inhibition, the need to discover selective and reversible MAGL inhibitors remains urgent. To our knowledge, the only compounds described as good reversible MAGL inhibitors are the naturally occurring terpenoids **pristimerin** and **euphol** (Figure 1).¹³ However, these two compounds act on a large number of secondary targets and this makes their use and study as MAGL inhibitors very difficult.^{14,15} Very recently, the reversible MAGL inhibitor benzo[*d*][1,3]dioxol-5-ylmethyl 6-phenylhexanoate **3** (compound c21, Figure 1) was tested *in vivo* using the experimental allergic encephalomyelitis (EAE) mouse model, which is broadly studied as an animal model of human CNS demyelinating diseases, including multiple sclerosis and acute disseminated encephalomyelitis.¹⁶ This molecule was able to ameliorate the clinical progression of the multiple

1
2
3 sclerosis mouse model and, very importantly, the therapeutic effects were not accompanied by
4
5 catalepsy or other motor impairments that have been observed after the administration of
6
7 irreversible MAGL inhibitors, thus supporting the hypothesis that reversible inhibitors could be
8
9 profitably used in *in vivo* models.¹⁶
10

11
12 We have recently reported a virtual screening study for the discovery of new reversible MAGL
13
14 inhibitors. Among the tested compounds, (4-(4-chlorobenzoyl)piperidin-1-yl)(4-
15
16 methoxyphenyl)methanone **4** (CL6a, Figure 2) proved to be an interesting reversible MAGL
17
18 inhibitor lead due to its inhibition activity ($K_i = 8.6 \mu\text{M}$ and $\text{IC}_{50} = 11.7 \mu\text{M}$), the absence of
19
20 stereocenters in its structure and its good synthetic accessibility.¹⁷ With the aim of identifying
21
22 potent and selective MAGL inhibitors, chemical modifications guided by molecular modeling
23
24 predictions of the probable binding poses were made to the structure of the initial compound **4** as a
25
26 first step of our attempt to improve the inhibition potency of **4** on MAGL. The synthesis of new
27
28 analogues of **4**, their biological characterization on the isolated enzyme as well as their
29
30 antiproliferative activities on a series of cancer cells are reported in this study.
31
32
33
34

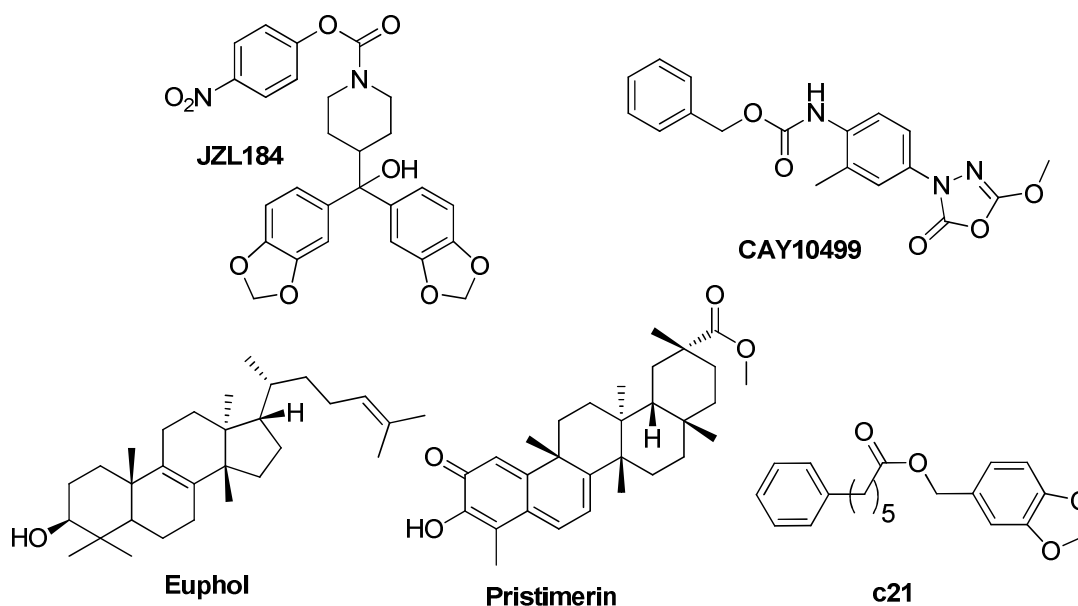


Figure 1. Structures of known MAGL inhibitors.

RESULTS AND DISCUSSION

Design and Molecular Modeling. As shown in Figure 2, by using a plane that divides the piperidine ring we can observe that compound **4** is symmetrical, with the exception of the piperidine nitrogen atom and the different aryl substituents at the two opposite sides of the molecule (a chloro atom in position 4 of the phenyl ring of the ketone side and a methoxy group in the same position of the phenyl ring of the amidic portion).

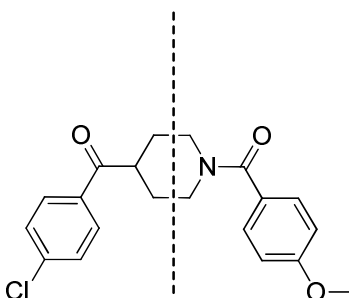
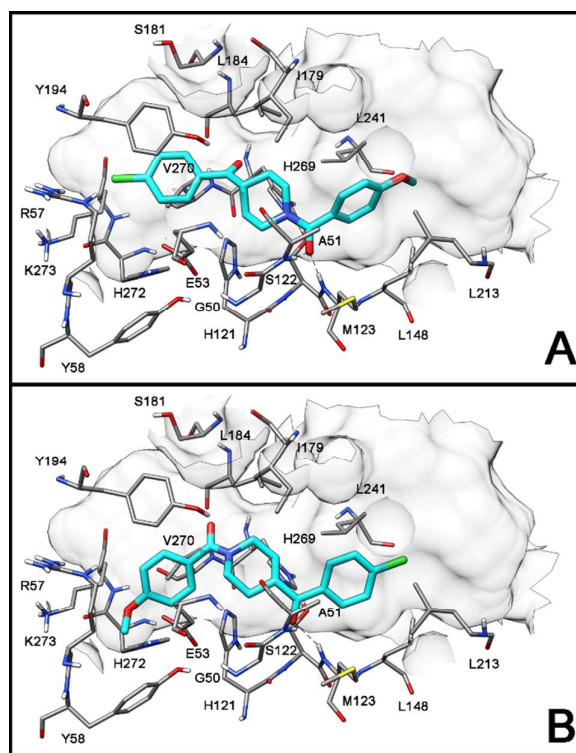


Figure 2. 2D analysis of compound **4**.

Before proceeding with the synthesis of **4** analogues, an extensive docking analysis was carried out in order to establish the binding disposition of this ligand. Figure S1 shows the clustering analysis of the docking results. This plot highlights the presence of two possible binding dispositions of the ligand, as there are two highly populated clusters of docking poses with very similar energy interaction scoring values. The most energetically favorable binding mode shows that the amidic C=O group of **4** forms two H-bonds with the nitrogen backbone of A51 and M123 and the 4-methoxyphenyl fragment is directed towards an open cavity of the protein showing lipophilic interactions with L148, L213 and L241. The 4-chlorobenzoyl moiety is inserted into a small pocket of the protein and shows lipophilic interactions of the phenyl ring with Y194 and V270 (binding mode A of Figure 3). Figure 3B shows a representative docking pose of the second cluster which is

1
2
3 more populated than the first one, but it shows a slightly lower energy interaction score. As
4
5 expected, this binding disposition is symmetrical to the first one: the 4-chlorobenzoyl moiety of the
6
7 **4** is directed towards the open cavity of the protein showing lipophilic interactions with L148, L213
8
9 and L241 and forms two H-bonds with the nitrogen backbone of A51 and M123. With regards to
10
11 the 4-methoxybenzoyl fragment, it is inserted into the small pocket of the protein and the phenyl
12
13 ring shows lipophilic interactions with Y194 and V270.
14
15
16



17
18
19
20
21
22
23
24
25
26
27
28
29
30
31
32
33
34
35
36
37
38
39
40
41
42
43 **Figure 3.** Docking of compound **4** into *hMAGL*. (A) Binding mode A; (B) binding mode B.
44
45
46
47

48
49 In order to identify which one is the preferred binding mode among the two proposed solutions by
50
51 the docking analysis (see Figure 3), we planned to synthesize two analogues of compound **4** that are
52
53 respectively able to adopt only one of these binding modes. In fact, biphenylic compounds **5** and **6**
54
55 (Table 1) were designed considering: a) the small volume of the pocket delimited by E53, R57,
56
57 Y58, Y194, V270 and H272, and b) the open shape of the cavity on the opposite side of the binding
58
59
60

1
2
3 site. These two compounds are characterized by the presence of a bulky biphenyl ring that we
4 hypothesized could lie only in the open cavity of the binding site surrounded by hydrophobic
5 residues L148, L213 and L241. As shown in Figure 4 and Figure S2, our hypothesis was confirmed
6
7
8
9
10
11
12
13
14
15
16
17
18
19
20
21
22
23
24
25
26
27
28
29
30
31
32
33
34
35
36
37
38
39
40
41
42
43
44
45
46
47
48
49
50
51
52
53
54
55
56
57
58
59
60

site. These two compounds are characterized by the presence of a bulky biphenyl ring that we hypothesized could lie only in the open cavity of the binding site surrounded by hydrophobic residues L148, L213 and L241. As shown in Figure 4 and Figure S2, our hypothesis was confirmed by the docking studies, since there was only one predicted binding disposition for each compound, with the biphenyl ring that was placed in the open cavity of the binding site. Due to this disposition, compound **5** shows the binding mode A, with the C=O amidic group forming two H-bonds with the backbone N-H of A51 and M123. Conversely, compound **6** shows the binding mode B, with the ketone group that forms two H-bonds with the backbone nitrogen of A51 and M123.

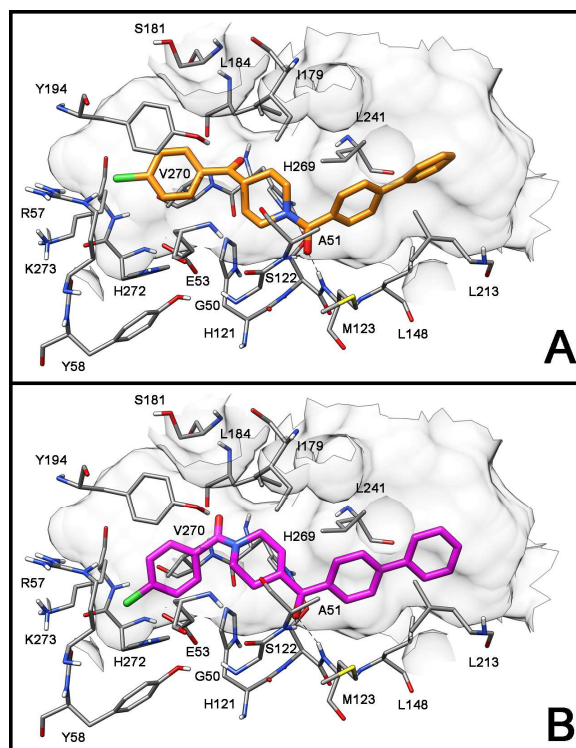
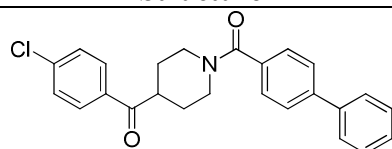
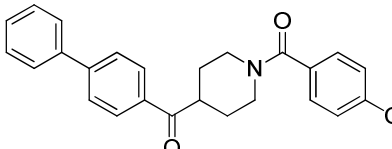
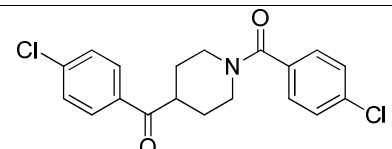


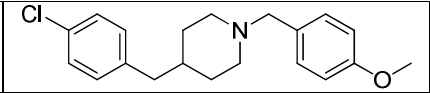
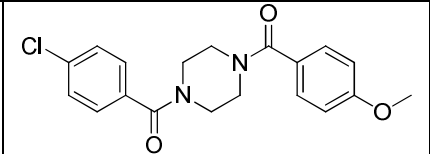
Figure 4. Docking results of compound **5** (A) and **6** (B) into *hMAGL*.

The two compounds were thus synthesized and tested for their *hMAGL* inhibition activity together with the piperidine-1,4-diylbis((4-chlorophenyl)methanone) derivative (**7a**, Table 1), which was

used as a reference compound, since it possesses the *para*-chloro substituted phenyl ring on both sides of the molecule, without the bulky biphenyl part that is present in the amidic portion of compound **5** or in the ketone moiety of compound **6**. As shown in Table 1, in agreement with the docking results, both binding modes are possible since both compounds show inhibition of MAGL activity. However, the binding mode B is the preferred one, since compound **6** shows a 5-fold higher activity ($IC_{50} = 2.1 \mu M$) than that of compound **5** ($IC_{50} = 9.9 \mu M$). Subsequently, two derivatives of compound **4** were synthesized and tested for their *h*MAGL inhibition activity in order to inspect the role of the central scaffold (Table 1). Compound **8**, which is characterized by the replacement of the two C=O groups with two methylene moieties, showed a complete loss of inhibition activity (IC_{50} greater than $100 \mu M$). Similar results were also obtained for compound **9**, which possesses a central piperazine ring instead of piperidine, thus introducing a second amidic group that further rigidifies the structure by reducing the rotational freedom of the *p*-chlorobenzoyl portion. Both results supported the important role of the central piperidine ring bearing a carbonyl group in the opposite position to the amidic fragment for the establishment of an efficient interaction with the enzyme, thus confirming the key role played by the central scaffold of **4**, which justifies the development of a series of analogues of this compound.

Table 1. Structure and *h*MAGL activity of compounds **5**, **6**, **7a**, **8** and **9**.

#	Structure	IC_{50} (μM)
5		9.9 ± 0.6
6		2.1 ± 0.4
7a		5.4 ± 0.1

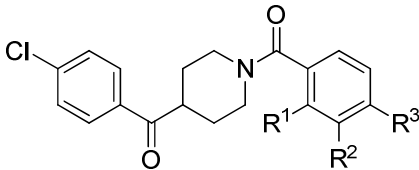
8		> 100
9		> 100

Hence, once we identified the preferred binding mode of this class of compounds into *h*MAGL, we proceeded with the lead optimization of **4**. As a first step in the development of this scaffold, we decided to improve the interaction of the compound inside the small pocket delimited by E53, R57, Y58, Y194, V270 and H272 while maintaining the rest of the molecule fixed. On this basis, we replaced the *p*-methoxyphenyl ring present in the amidic portion of the initial compound **4** with differently substituted aryl groups and kept the *p*-chlorobenzoyl unit fixed. Hence, we explored the *ortho/meta/para* effects generated by the presence in the amidic phenyl ring of halogen atoms (F, Cl, Br, I), methyl, trifluoromethyl, methoxy, trifluoromethoxy, hydroxy, amino and nitro substituents, by testing the inhibitory activities of the series of novel compounds reported in Table 2.

Enzymatic experiments. The inhibitory effects of the newly synthesized compounds on human isoforms of MAGL by using 4-nitrophenylacetate substrate are reported in Table 2, together with those of the reference irreversible inhibitor **1** and of the recently reported reversible inhibitor **3**. Considering the activity of compound **20** ($IC_{50} = 6.5 \mu\text{M}$), which possesses an unsubstituted phenyl ring, the introduction in all the three *o/m/p* positions of the aromatic ring of bromine and iodine (compounds **11a-c** and **12a-c**) determined an increase of the activity (IC_{50} values in the range 2.4-4.8 μM). The presence of the other substituents generally led to a certain reduction of inhibition activity, which resulted to be either lower than that of reference compound **20** (IC_{50} values in the range 9.9-57.3 μM) or comparable ($IC_{50} = 5.4 \mu\text{M}$ for **7a**, $IC_{50} = 7.1 \mu\text{M}$ for **13c**). It is worth noting

that almost all the reported compounds show an activity that is similar or even better than that of the reference reversible inhibitor **3**.

Table 2. Structures and *h*MAGL inhibitory activities of the synthesized compounds.



Compounds	R ¹	R ²	R ³	IC ₅₀ (μM)
7a	H	H	Cl	5.4 ± 0.7
7b	H	Cl	H	17.1 ± 0.1
7c	Cl	H	H	10.4 ± 0.5
10a	H	H	F	17.8 ± 0.9
10b	H	F	H	20.4 ± 0.1
10c	F	H	H	13.4 ± 0.6
11a	H	H	Br	2.4 ± 0.1
11b	H	Br	H	4.8 ± 0.4
11c	Br	H	H	4.0 ± 0.4
12a	H	H	I	4.4 ± 0.2
12b	H	I	H	4.3 ± 0.4
12c	I	H	H	2.4 ± 0.2
13a	H	H	CH ₃	11.8 ± 0.4
13b	H	CH ₃	H	10.9 ± 0.8
13c	CH ₃	H	H	7.1 ± 0.1
14a	H	H	CF ₃	29.8 ± 1.3
14b	H	CF ₃	H	11.9 ± 0.4
14c	CF ₃	H	H	26.3 ± 2.4
4	H	H	OCH ₃	11.7 ± 2.2
15b	H	OCH ₃	H	9.9 ± 1.7
15c	OCH ₃	H	H	11.5 ± 0.3
16a	H	H	OCF ₃	26.6 ± 2.6
16b	H	OCF ₃	H	16.3 ± 1.0
16c	OCF ₃	H	H	17.3 ± 1.2
17a	H	H	OH	11.7 ± 1.7
17b	H	OH	H	0.84 ± 0.04
17c	OH	H	H	32.8 ± 4.3
18a	H	H	NH ₂	16.7 ± 1.7
18b	H	NH ₂	H	57.3 ± 2.2
18c	NH ₂	H	H	15.5 ± 1.9
19a	H	H	NO ₂	14.2 ± 0.3
19b	H	NO ₂	H	24.9 ± 3.5
19c	NO ₂	H	H	24.0 ± 0.4
20	H	H	H	6.5 ± 0.1
1				0.048 ± 0.005

2	0.134 ± 0.015
3	9.0 ± 1.5

Among the 34 reported derivatives, the *m*-hydroxy-substituted derivative **17b** showed a high inhibition activity ($IC_{50} = 0.84 \mu\text{M}$), about 14 fold more potent than the starting **4** lead compound. In order to better rationalize the activity of this compound, **17b** was subjected to docking calculations, together with its analogues **17a** and **17c**. Binding mode B of compound **17b** resulted to be more energetically favorable than the other one (see Figure S3). The overall disposition of the molecule is comparable to that observed for compound **4**, with the 4-chlorobenzoyl moiety that is directed towards the open cavity of the protein showing lipophilic interactions with L148, L213 and L241 and the formation of two H-bonds with the backbone nitrogen of A51 and M123 (see Figure 5). The *m*-hydroxybenzoyl fragment is inserted into the small pocket of the protein and shows lipophilic interactions between its aryl ring and residues Y194 and V270. Furthermore, the *m*-hydroxyl participates to a highly energetic H-bond network with residues E53 and H272, where it behaves as a H-bond acceptor with H272 and as a H-bond donor with E53. It is interesting to note that, analyzing the main crystal structures of *h*MAGL¹⁸⁻²¹ and superimposing them with the *h*MAGL-**17b** complex, the hydroxyl group of the ligand replaces a structural water molecule that acts as a H-bond bridge between E53 and H272, thus supporting the high activity of this compound (see Figure S4). The replacement of the *m*-hydroxyl with the *o*- and *p*-hydroxyl group determined a marked decrease of the MAGL inhibition activity (see compounds **17c** and **17a**, respectively). As shown in Figure S5, the docking results suggested that for both compounds the shift of the hydroxyl group from the *meta* to *para* and *ortho* position determines the loss of the H-bonds with E53 and H272, without establishing any further interaction.

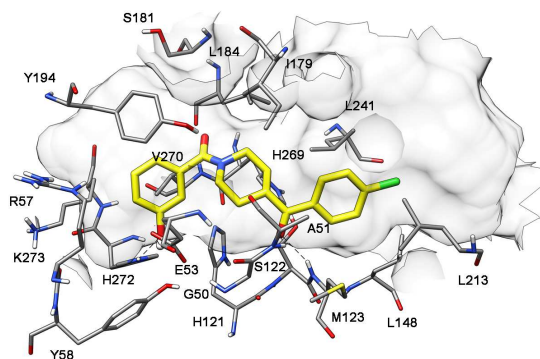


Figure 5. Docking results of compound **17b** into *hMAGL*.

The replacement of the *m*-hydroxy with the *m*-amine group led to a marked decrease of activity (compound **18b**, $IC_{50} = 57.3 \mu M$). Due to the planar geometry of the aniline nitrogen atom and to the delocalization of its electron lone pair in the adjacent π -system, it is unlikely that this group is able to act as a H-bond acceptor, thus supporting the low activity of this compound.

With the aim of evaluating the reversible or irreversible mechanism of inhibition, the effects of dilution and preincubation on the inhibitory ability of compound **17b** and of reference compounds **2** and **3** were evaluated. In the dilution experiments, if the compound is an irreversible inhibitor, then its inhibition potency should not drop upon dilution, whereas inhibition levels should be substantially reduced upon dilution in the presence of a reversible inhibitor. As shown in Figure 6, **17b** showed reversible inhibition, since the inhibition produced by 20 μM of the compound was significantly higher compared with that observed with a 40X dilution, which appears similar to that produced by a 0.5 μM concentration of the compound. The same results were also obtained for compound **3**, whereas compound **2** showed an irreversible inhibition since the inhibition produced by 4 μM of the compound was substantially unchanged upon a 40X dilution, which appears significantly higher to that produced by a 0.1 μM concentration of this compound.

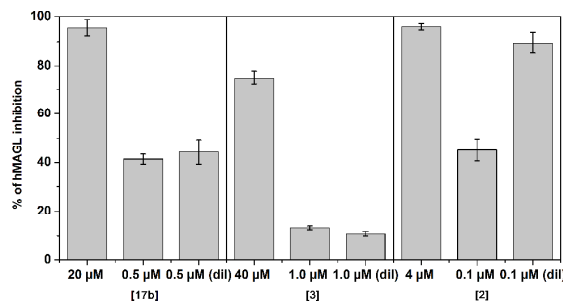


Figure 6. Dilution assay for compounds **17b**, **3** and **2**: the first two columns indicate the inhibition percentage of compounds at a concentration of 20 μ M and 0.5 μ M (**17b**), 40 μ M and 1.0 μ M (**3**) and 4 μ M and 0.1 μ M (**2**). The third column indicates the inhibition percentage of compounds after a 40X dilution (final concentration = 0.5 μ M, 1.0 μ M and 0.1 μ M for compounds **17b**, **3** and **2**, respectively).

In order to further support these results, the activity of **17b**, **2** and **3** were tested at different preincubation times of the inhibitors with the enzyme. An irreversible inhibitor will increase its ability to block MAGL over gradually longer incubation times. On the contrary, unchanged IC_{50} values in these experiments support a reversible mechanism of action.²² As expected, compound **17b** and **3** showed a constant MAGL inhibition activity even after 60 min of preincubation, thus supporting a reversible mode of action (see Figure 7). As expected, instead, a time-dependent increase of potency was observed for reference compound **2**, which further supports its already known irreversible inhibitor character.⁵

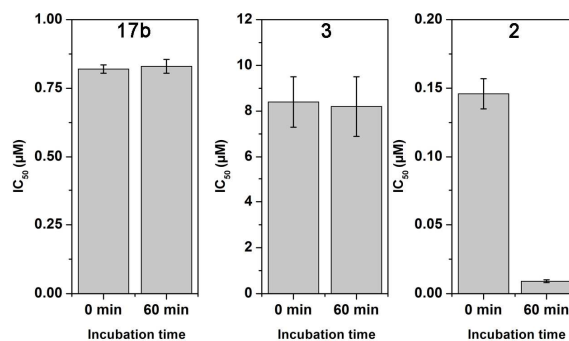


Figure 7. IC₅₀ (µM) values of **17b**, **3** and **2** at different preincubation times with *h*MAGL (0 min and 60 min).

Once we confirmed the reversibility of the inhibitory action of compound **17b**, we then evaluated its inhibition mode by measuring Michaelis–Menten kinetics. The dataset was plotted as substrate concentration *versus* enzyme activity and analyzed by applying the mixed-model inhibition fit of GraphPad Prism 5.0. This model, beyond the V_{\max} and K_m values, also calculates the α parameter, which can be useful for establishing the inhibition mechanism. Its value is greater than zero and determines the extent to which the binding process of the inhibitor changes the affinity of the enzyme for the substrate. If the inhibitor does not modify the binding of the substrate to the enzyme, α is equal to one and the mixed-model corresponds to a noncompetitive inhibition. When α is a very large value, the binding of the inhibitor prevents that of the substrate and the mixed-model corresponds to a competitive inhibition. Finally, when α is a very small value, the binding of the inhibitor increases the binding of the substrate to the enzyme, and the mixed-model corresponds to an uncompetitive model. Kinetic studies indicate for **17b** a K_i value of 0.65 ± 0.05 µM and an α value greater than 10000, thus suggesting a competitive binding for this compound (Figure 8).

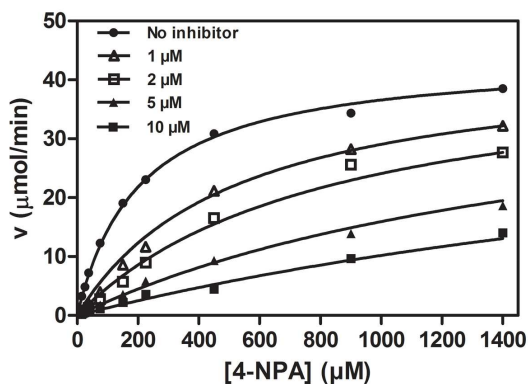


Figure 8. Michaelis–Menten plot for the determination of the K_i of compound **17b** for *h*MAGL ($K_i = 0.65 \pm 0.05 \mu\text{M}$, $\alpha > 10000$).

As a further analysis, in order to explore the potential activity of these compounds for other hydrolases, the selectivity *versus* the analogue enzyme fatty acid amide hydrolase (FAAH) of some of the most promising inhibitors was evaluated. As shown in Table 4, all the tested compounds showed MAGL selectivity. In particular, compound **17b** displayed a MAGL selectivity greater than 119-fold.

Table 4. MAGL selectivity *versus* FAAH for the best compounds.

Compd	MAGL IC_{50} (μM)	FAAH IC_{50} (μM)	Selectivity Index
11b	4.8 ± 0.4	> 100	> 21
12c	2.4 ± 0.2	86.7 ± 5.1	36
13c	7.1 ± 0.2	> 100	> 14
17b	0.84 ± 0.04	> 100	> 119
3	9.0 ± 1.5	27.7 ± 1.1	3

1
2
3 **Molecular dynamic simulation.** In order to evaluate the reliability of the docking results and to
4 carry out an analysis of the ligand–protein interaction, the *h*MAGL-**17b** complex was used as a
5 starting structure for 51 ns of molecular dynamic (MD) simulation. As shown in Figure S6, the
6 complex is stable during the simulations and the analysis of the root-mean-square deviation (rmsd)
7 of all the heavy atoms from the X-ray structures highlights a stabilization of the rmsd value around
8 0.8 Å. With regard to the geometry of the compounds, analyzing the rmsd of the position of the
9 ligand during the simulations with respect to the starting structure, it maintains its starting
10 disposition with an rmsd value between 0.3 and 0.7 Å. With regard to the H-bond analysis (Table
11 S1 in the Supporting Information), the interaction of the hydroxyl group with E53 and H272
12 appears to be very stable, similarly to the interaction with the nitrogen backbone of A51. Differently
13 from what reported in the docking studies, the interaction with the backbone nitrogen of M123 is
14 not highly conserved; however, this is due to a small shift of the ligand with the formation of a very
15 stable H-bond between the hydroxyl group of S181 and the amidic oxygen of the compound (see
16 Figure S7).

17
18
19
20
21
22
23
24
25
26
27
28
29
30
31
32
33
34 **Antiproliferative assays.** Compound **17b** was also further tested in *in vitro* experiments for
35 evaluating its antiproliferative activity against cancer cells. Compound **2** and **3** were used as
36 reference compounds. Due to the potential role of MAGL as a therapeutic target in ovarian cancer,²³
37 four human ovarian cancer cell lines (OVSAHO, OVCAR3, COV318 and CAO3) were chosen
38 and a western blot analysis was carried out in order to measure the overexpression of MAGL in
39 these cells. As shown in Figure 9A, western blot analysis highlighted an overexpression of MAGL
40 in OVCAR3 and CAO3 compared to OVSAHO and COV318 cell lines. Compound **17b** caused a
41 considerable inhibition of cell viability, with IC₅₀ values ranging from 31.5 to 43.9 μM in the
42 OVCAR3 and CAO3 cell lines (Table S2), whereas it proved to be remarkably less potent against
43 ovarian cancer cells that do not overexpress MAGL, such as OVSAHO and COV318 cells.
44 Furthermore, **17b** proved to be completely inactive also against noncancerous human fibroblast
45
46
47
48
49
50
51
52
53
54
55
56
57
58
59
60

lung cells (MRC5, Figure 9B). Differently, the covalent reference inhibitor **2** showed inhibition of cell viability in all the four ovarian cancer cell lines, with IC_{50} values ranging from 17.2 to 83.1 μM (Table S2). This behavior may be due to the lack of target-selectivity of this compound, thus we cannot exclude that the involvement of different targets could contribute to its antiproliferative potential. Surprisingly, the known MAGL inhibitor **3** displayed a substantial inactivity against all the tested cell lines. Overall, these data suggest that the reversible inhibition of MAGL operated by the herein reported class of compounds may be a possible profitable alternative to the irreversible inhibition treatment.

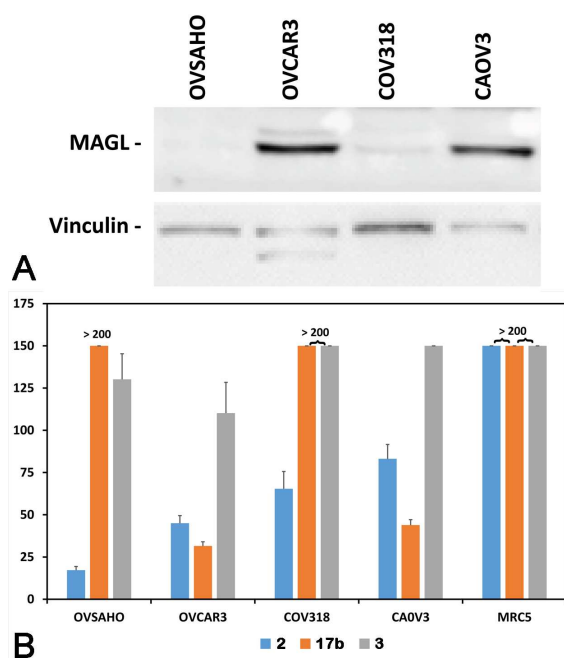
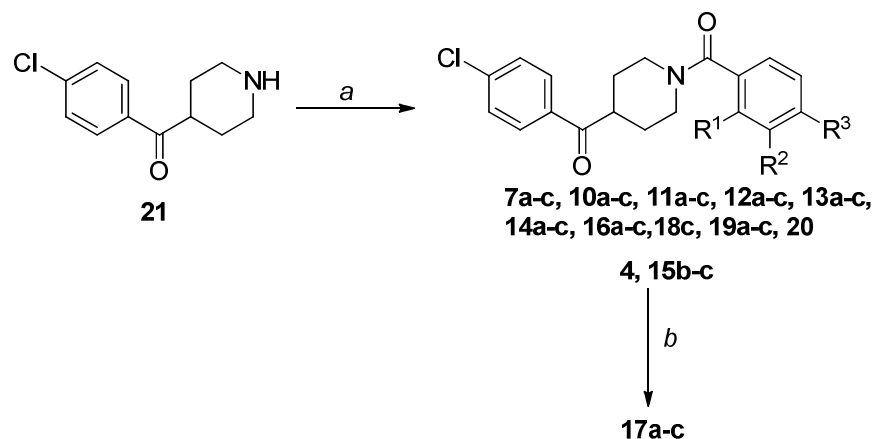


Figure 9. A) Western blot analysis of MAGL expression in ovarian cancer cell lines. Vinculin was utilized to normalize the amount of total loaded proteins. B) Cell growth inhibitory activities (IC_{50}) of compounds **2**, **17b** and **3**.

1
2
3 **Chemistry.** Benzoyl piperidine derivatives **4**, **7a-c**, **10a-c**, **11a-c**, **12a-c**, **13a-c**, **14a-c**, **15b-c**, **16a-c**,
4
5 **19a-c** and **20** were synthesized by an amide coupling between properly substituted benzoic acids
6
7 and 4-(4-chlorobenzoyl)piperidine **21** in the presence of the condensing agent HATU and DIPEA as
8
9 the base in dry *N,N*-dimethylformamide as the solvent, as previously reported for compound **4**.¹⁷
10
11 Hydroxy-substituted derivatives **17a-c** were obtained after BBr₃-promoted deprotection of the
12
13 corresponding methoxylated precursors **4**, **15b-c**. A particular case was the *ortho*-amino substituted
14
15 compound **18c** which, unlike its analogues *para*- and *meta*-NH₂-bearing compounds **18a-b** (see
16
17 Scheme 2), was directly obtained from condensation of 4-(4-chlorobenzoyl)piperidine with
18
19 anthranilic acid (Scheme 1), since the protection of the amino moiety with *tert*-butyloxycarbonyl
20
21 group, similarly adopted for the *para*- and *meta*-analogues, needed very long reaction times with the
22
23 simultaneous formation of many side-products, therefore the direct condensation was preferred,
24
25 although this caused a decrease in the reaction yield,
26
27
28
29

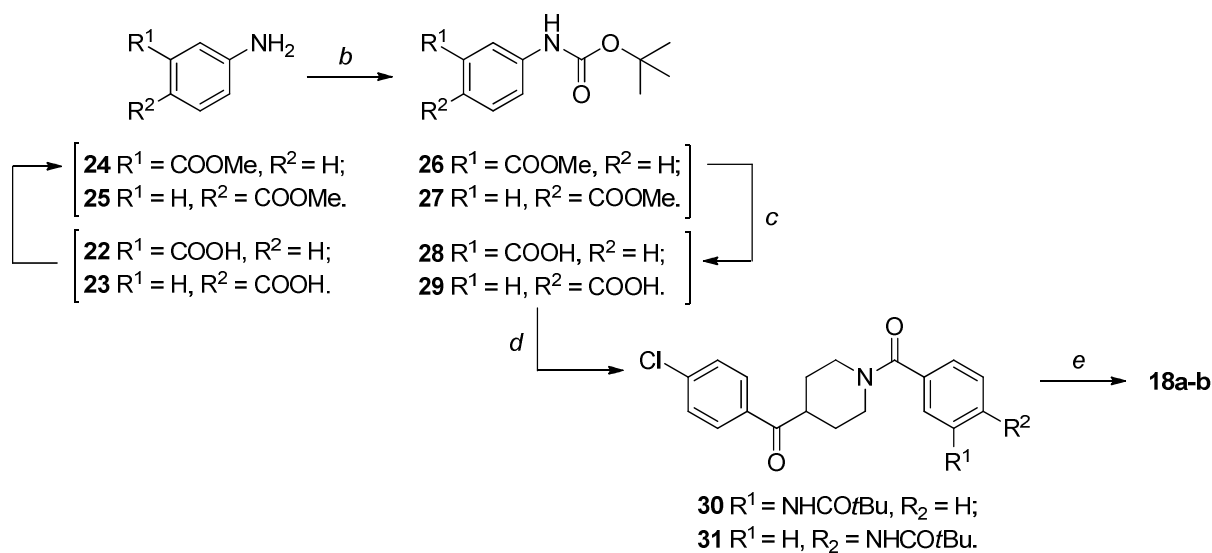


47 **Scheme 1. Synthesis of benzoyl-piperidine derivatives.**^a

48 ^aReagents and conditions: (a) properly substituted benzoic acid (1 eq), HATU (1.05 eq), DIPEA (4
49 eq), dry DMF, RT, 6-8 h; (b) 1M BBr₃, dry CH₂Cl₂, -78 to 0 °C, then RT, 1-2 h.

50
51
52
53
54 As anticipated in the previous discussion, the synthesis of amino-substituted compounds **18a-b**
55
56 started with the formation of the methyl esters **24** and **25** from the corresponding amino-benzoic
57
58 acids **22** and **23** by refluxing them in MeOH in the presence of SOCl₂ (Scheme 2). Boc-protection
59
60

of the amino groups with di-*tert*-butyl dicarbonate in the presence of triethylamine in THF gave compounds **26** and **27**, which were then hydrolyzed to give Boc-protected benzoic acids **28** and **29** ready to be condensed with piperidine **21**. The amino groups of the intermediate amides **30** and **31** were finally deprotected by reaction with trifluoroacetic acid in DCM to obtain compounds **18a** and **18b** in good yields.

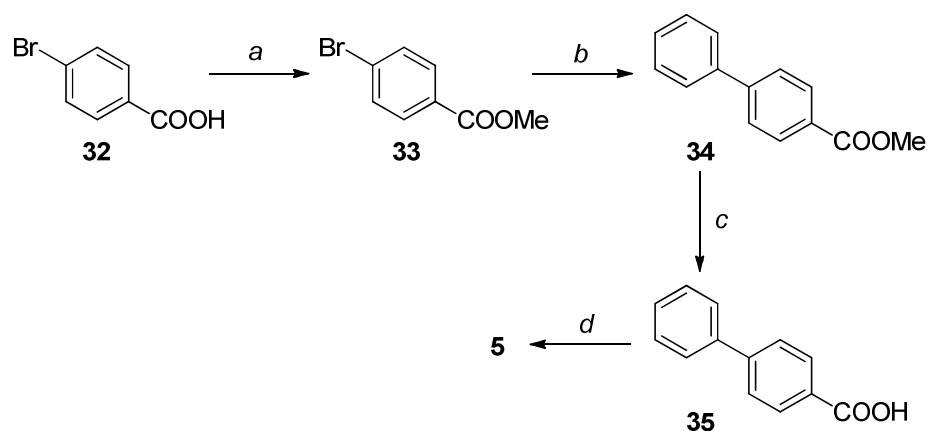


Scheme 2. Synthesis of *meta* and *para*-amino-substituted benzoyl-piperidine derivatives **18a-b.^a**

^aReagents and conditions: *a*) MeOH, SOCl₂ (2.5 eq), reflux, 3 h; *b*) (Boc)₂O (2 eq), Et₃N (2 eq), dry THF, RT, 24 h; *c*) aq. 2N LiOH (6 eq), THF/MeOH 1:1 v/v, RT, overnight; *d*) (4-chlorophenyl)(piperidin-4-yl)methanone **21** (1 eq), HATU (1.05 eq), DIPEA (4 eq), dry DMF, RT, 3-4 h; *e*) CF₃COOH, dry DCM, 0 °C to RT, 3-5 h.

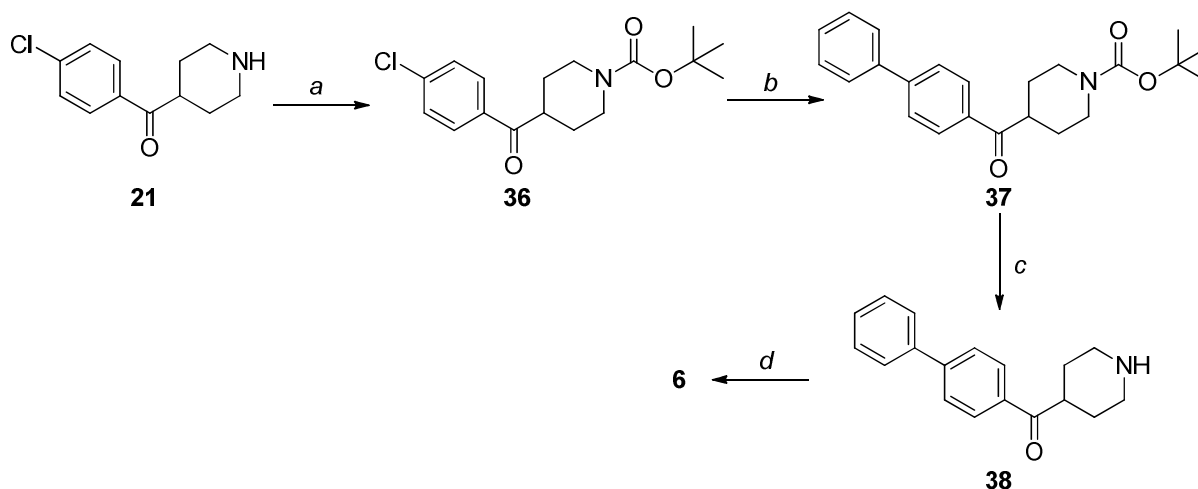
The synthetic approaches for the synthesis of the biphenyl derivatives **5** and **6** are reported in Schemes 3 and 4. For the synthesis of compound **5**, [1,1'-biphenyl]-4-carboxylic acid **35** was obtained after a sequence of reactions starting from 4-bromobenzoic acid **32**, consisting in a Fischer esterification to obtain the methyl ester **33**, followed by a palladium-catalyzed cross-coupling reaction to replace the bromine atom with a phenyl ring. This step required anhydrous conditions to

1
2
3 prevent the hydrolysis of the methyl ester group under prolonged heating in the presence of alkaline
4 solutions, since the isolation and purification of the biphenyl methyl ester was preferred. Finally,
5 hydrolysis of the methyl ester gave compound **35** which was condensed with 4-(4-
6 chlorobenzoyl)piperidine **21** in the presence of HATU and DIPEA to yield the desired compound.
7
8
9
10
11 The synthesis of compound **6** started with the protection of piperidine **21**, then a cross-coupling
12 reaction adopting the Fu-type conditions, which are suitable for the coupling of aryl chlorides with
13 the appropriate phenylboronic acid, using the catalytic system containing Pd₂(dba)₃ and
14 tricyclohexylphosphine, and cesium carbonate as the base, gave compound **37**. TFA-promoted
15 deprotection of the piperidine *N*-atom gave compound **38**, which was reacted with 4-chlorobenzoic
16 acid in the same conditions adopted for all the amidic condensation of this class of compounds to
17 produce compound **6** in high yields.
18
19
20
21
22
23
24
25
26



42 **Scheme 3. Synthesis of biphenyl derivative 5.^a**

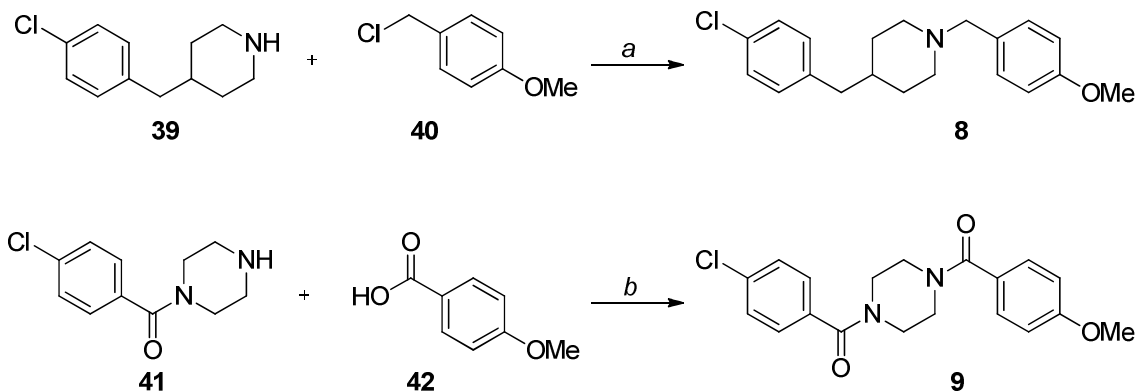
43
44 ^aReagents and conditions: (a) MeOH, H₂SO₄, reflux, overnight; (b) PhB(OH)₂ (2 equiv), Pd(OAc)₂
45 (0.03 eq), PPh₃ (0.15 eq), K₂CO₃ (1.5 eq), toluene, 100 °C, 18 h; (c) aq. 2N LiOH (6 eq),
46 THF/MeOH 1:1 v/v, RT, 20 h; (d) (4-chlorophenyl)(piperidin-4-yl)methanone **21** (1 eq), HATU
47 (1.05 eq), DIPEA (4 eq), dry DMF, RT, 3 h.
48
49
50
51
52
53
54
55
56
57
58
59
60



Scheme 4. Synthesis of biphenyl derivative 6.^a

^aReagents and conditions: (a) (Boc)₂O (1.2 eq), Et₃N (2 eq), dry THF, RT, 2 h; (b) PhB(OH)₂ (1.6 equiv), Pd₂(dba)₃ (0.032 eq), Cy₃P 20% toluene (0.08 eq), Cs₂CO₃ (1.7 eq), dioxane, 100 °C, overnight; (c) CF₃COOH, dry DCM, 0 °C to RT, 2 h; (d) 4-chlorobenzoic acid (1 eq), HATU (1.05 eq), DIPEA (4 eq), dry DMF, RT, 6 h.

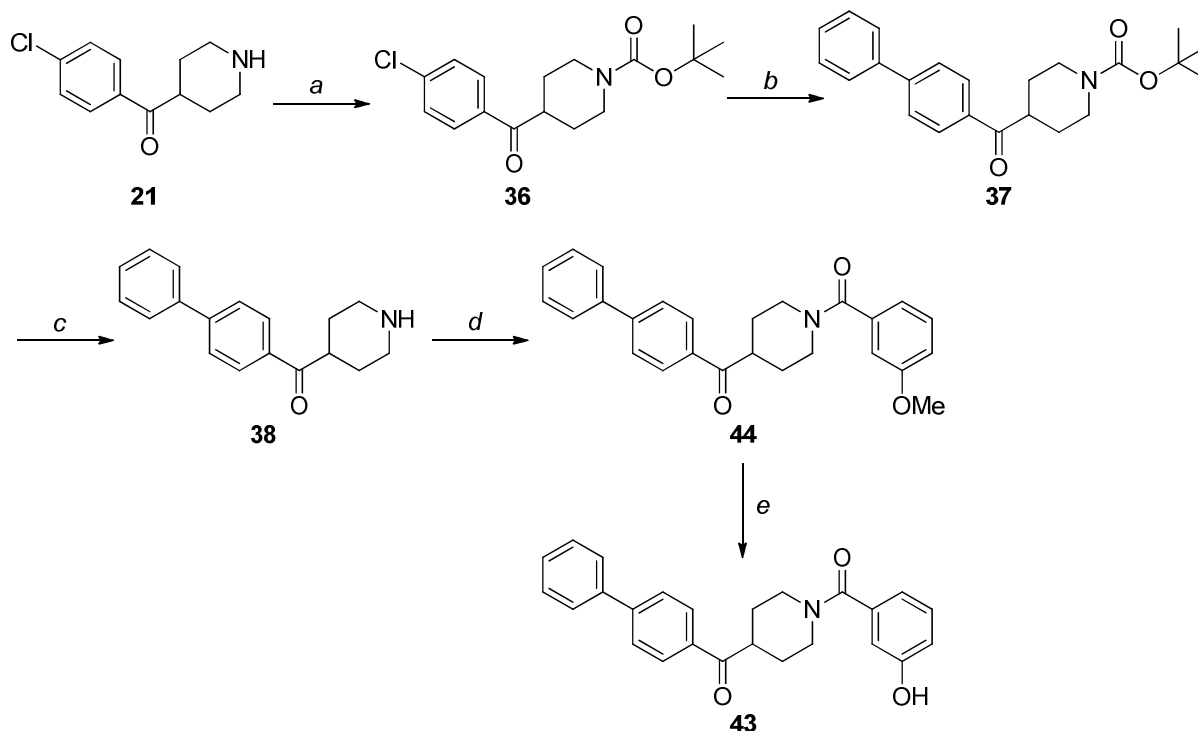
The synthesis of compounds **8** and **9** is reported in Scheme 5 and for both derivatives a one-pot procedure gave the desired products. Derivative **8** was obtained by alkylation of 4-(4-chlorobenzyl)piperidine hydrochloride **39** with 4-methoxybenzyl chloride **40** using potassium carbonate as the base. Differently, the amidic condensation between 1-(4-chlorobenzoyl)piperazine **41** and 4-methoxybenzoic acid **42** under the same conditions previously described for the synthesis of other compounds (Schemes 1-4) gave derivative **9**.



1
2
3 **Scheme 5. Synthesis of compounds 8 and 9.^a**
4

5 ^aReagents and conditions: (a) an. K₂CO₃ (3 eq.), dry DMF, RT, overnight; (b) HATU (1.05 eq),
6
7 DIPEA (4 eq), dry DMF, RT, 3 h.
8
9

10
11 For the synthesis of compound **43** (see Conclusions section), the synthetic scheme described for the
12 preparation of biphenylic piperidine **38** (Scheme 4) was adopted, then piperidine **38** was submitted
13 to a condensation with 3-methoxybenzoic acid to get amide **44**, followed by deprotection of the
14 methoxy group with boron tribromide, to obtain the final compound **43** (Scheme 6).
15
16
17
18
19



Scheme 6. Synthesis of compound 43.^a

^aReagents and conditions: (a) (Boc)₂O (1.2 eq), Et₃N (2 eq), dry THF, RT, 2 h; (b) PhB(OH)₂ (1.6
equiv), Pd₂(dba)₃ (0.032 eq), Cy₃P 20% toluene (0.08 eq), Cs₂CO₃ (1.7 eq), dioxane, 100 °C,
overnight; (c) CF₃COOH, dry DCM, 0 °C to RT, 2 h; (d) 3-methoxybenzoic acid (1 eq), HATU
(1.05 eq), DIPEA (4 eq), dry DMF, RT, 4 h; (e) 1M BBr₃, dry CH₂Cl₂, -78 to 0 °C, then RT, 1 h.

1
2
3 A detailed analysis of ^1H and ^{13}C -NMR spectra of some (1-benzoylpiperidin-4-yl)(4-
4 chlorophenyl)methanone derivatives revealed the presence of two rotational conformers generated
5 by the rotation of the bond between the variously substituted phenyl ring and the amidic carbonyl
6 group. The splitting of ^1H and ^{13}C -NMR signals was observed for *ortho*-substituted compounds,
7 since the presence of bulky groups in this position such as Cl (**7c**), Br (**11c**), I (**12c**), CF_3 (**14c**), CH_3
8 (**13c**), OCH_3 (**15c**), and OCF_3 (**16c**) led to the presence of two rotational conformers. Conversely
9 when the substituents are either absent or are present in *meta* or *para* positions the rotation is free at
10 room temperature and a unique conformer is observed by NMR analysis. In the case of compounds
11 **17c** and **18c**, the presence of *ortho*-OH (**17c**) or *ortho*- NH_2 (**18c**) groups allows the formation of an
12 intramolecular H-bond between the hydrogen atom of hydroxyl or amino group and the amide $\text{C}=\text{O}$
13 oxygen atom, thus inducing a stabilization of only one conformer. Surprisingly, for *ortho*-fluoro
14 derivative **10c** no splitting of signals was observed, despite the non-negligible steric hindrance of
15 the halogen atom. This observation may be explained considering the partial negative charge of
16 both the fluorine atom and the carbonyl oxygen atom, which cause a charge repulsion leading to the
17 stabilization of the conformer where these two atoms maximize their distance. Similarly, the single
18 conformer observed for the *ortho*-nitro derivative **19c** may have the nitro group and the carbonyl
19 oxygen atom distant, due to the repulsion between the partially negatively charged oxygen of the
20 amide $\text{C}=\text{O}$ and the negatively charged oxygens of the NO_2 group, causing the block of the rotation
21 which leads to the presence of a single conformer. The presence of conformer was verified for a
22 representative compound, (4-(4-chlorobenzoyl)piperidin-1-yl)(2-iodophenyl)methanone **12c**, by
23 acquiring ^1H -NMR spectrum at high temperature (80 °C) in a suitable solvent ($\text{DMSO}-d_6$), in order
24 to overcome the energetic rotational barrier for the different conformers and thus collapse the
25 splitting of signals. As shown in Figures S8-S10, the high temperature increased the interconversion
26 rate between the two rotamers and the spectrum revealed a collapse of the signals of the two
27 conformers, which is particularly evident in the aromatic region of the spectrum.
28
29
30
31
32
33
34
35
36
37
38
39
40
41
42
43
44
45
46
47
48
49
50
51
52
53
54
55
56
57
58
59
60

CONCLUSIONS

In summary, molecular modeling predictions of the probable binding pose guided chemical modifications of the structure of the initial compound **4** as a first attempt to improve the inhibition potency of this compound on *h*MAGL. The first part of the structural optimization of **4** led to the identification of compound **17b**, which displayed remarkably high MAGL inhibition activity, selectivity for MAGL over FAAH, reversible interaction properties and antiproliferative activity in cancer cells. Therefore, to the best of our knowledge **17b** can now be considered as one of the most active reversible MAGL inhibitors ever reported so far in literature. Finally, the *m*-hydroxyl substituent of this compound replaces a structural water molecule present in the main crystal structures of *h*MAGL.¹⁸⁻²¹ Considering that almost all the known MAGL inhibitors show H-bond interactions only in the proximity of the oxyanion hole, constituted by the backbone NH groups of A51 and M123, the possibility of replacing a water molecule by forming profitable H-bonds also with E53 and H272 residues could provide a new key anchoring point for the development of new MAGL inhibitors. As a further attempt to improve the MAGL inhibition activity of the reported compounds, the replacement of the *p*-chlorophenyl group of compound **17b** with fragments that are characterized by different size and interaction points is currently underway. In the present paper we have modified only the amidic phenyl portion of the scaffold with the insertion of simple and small groups as a first-stage optimization study. It is our purpose now to carry out further modifications of the structure of the best compound **17b**, with the aim of obtaining derivatives that are characterized by an improved MAGL inhibition activity. As a preview of our future optimization work, we have observed that the replacement of the *p*-chlorophenyl ring with a biphenyl ring (compound **6**) leads to about a two-fold increase of activity (compared to compound **7a**). Therefore, as a preliminary attempt to improve the activity of compound **17b**, we synthesized and tested the (4-([1,1'-biphenyl]-4-carbonyl)piperidin-1-yl)(3-hydroxyphenyl)methanone derivative (compound **43**, Scheme 6). As shown in Figure S13, in an agreement with the herein reported data, adding a second phenyl ring in

1
2
3 compound **43** led to a two-fold increase of activity with respect to **17b** ($IC_{50} = 0.46 \pm 0.02 \mu M$),
4
5 thus confirming the promising possibilities of further improving the inhibition activity of the best
6
7 derivative of this series of compounds by modifying the *p*-chlorophenyl region of the molecule.
8
9

10 EXPERIMENTAL SECTION

11 Pan Assay Interference Compounds (PAINS) analysis.

12
13
14 The herein reported class of compounds could act as artifacts and promiscuous bioactive molecules.
15
16 Therefore, a PAINS analysis for the most active compound (**17b**) was carried out in order to
17
18 analyze and exclude this possibility.
19
20

21
22 *PAINS substructural features screening.* Baell and Holloway published an interesting paper on the
23
24 analysis of frequent hitters from screening assays.²⁴ This report described a number of substructural
25
26 features which could help to identify compounds that appear as PAINS in many biochemical high
27
28 throughput screens. In the supplementary information they provided the corresponding filters that
29
30 have been included in the Filter-itTM software. Compound **17b** was thus filtered by using this
31
32 program and as a result it was recognized as no PAIN molecule because it did not possess any of
33
34 the substructural features shared by the most common PAINS.
35
36

37
38 *Interference analysis.* Some PAINS are associated with color that could interfere photometrically
39
40 with the assay. As reported in the part of MAGL inhibition assay of the Experimental Section, in
41
42 order to avoid this possibility for each compound concentration a blank analysis was carried out,
43
44 and the final absorbance values resulted from the subtraction of the absorbance determined by the
45
46 presence of all the components except the enzyme in the same conditions. Furthermore, a specific
47
48 analysis for compound **17b** was carried out. The 4-nitrophenylacetate (4-NPA) to 4-nitrophenol (4-
49
50 NP) conversion curve was prepared at 100 μM total concentration of 4-NPA+4-NP in the presence
51
52 and absence of **17b** at a concentration of 200 μM . As shown in the Figure S11, the two resulting
53
54 curves were superimposable. As a positive control, we analyzed in the same conditions the effects
55
56 of quercetin at 200 μM , that resulted in a shifted curve. Finally, we analyzed the results in the first
57
58
59
60

1
2
3 part of the plot, in the 100-80 μM concentration range of 4- NPA (corresponding to 0-20%
4 conversion of 4-NAP to 4-NP). As shown in Figure S11 the two straight lines measured in the
5 presence and absence of **17b** were almost identical, differently from what observed for quercetin,
6 that produced a shifted line, thus suggesting that **17b** did not interfere with the reading at 405 nm in
7 the enzymatic assay.
8

9
10
11
12
13
14 *Aggregation analysis.* All the enzymatic assays were carried out in the presence of bovine serum
15 albumin (BSA) 0.1 mg/ml. However, in order to further verify the possible formation of aggregates,
16 the MAGL inhibition activity of compound **17b** was also tested in the presence of 0.01% (v/v)
17 Triton X-100 as detergent. With respect to the IC_{50} value obtained in the presence of BSA ($\text{IC}_{50} =$
18 $0.84 \pm 0.04 \mu\text{M}$), a similar result was obtained ($\text{IC}_{50} = 0.76 \pm 0.02 \mu\text{M}$) in the presence of Triton X-
19 100, supporting the notion that the ligand is operating as a monomer rather than an aggregate.²⁵
20
21
22
23
24
25
26
27

28
29 *Thiol reactive analysis.* As reported by Walters and co-workers,²⁶ promiscuous enzymatic inhibition
30 could be due in some cases to covalent reaction with cysteines on multiple proteins. MAGL
31 inhibition activity of compound **17b** was also tested in the presence of the thiol-containing agent
32 1,4-dithio-DL-threitol (DTT).⁷ As shown in Figure S12, the MAGL- IC_{50} value of compound **17b**
33 was not influenced by the presence of DTT, as it showed a $\text{IC}_{50} = 0.80 \pm 0.05 \mu\text{M}$ when assayed
34 with 100 μM DTT, thus excluding the interaction of this compound with the cysteine residues of the
35 MAGL enzyme.
36
37
38
39
40
41
42
43
44

45
46 *Selectivity testing and orthogonal assay.* As reported by Dahlin and Walters²⁷ the selective activity
47 of a compound and the measurement of the activity against the target by using a different readout
48 method are two other steps that contribute to elucidate the PAINS properties. As reported in Table 4
49 we measured the activity of compound **17b** against FAAH and the results highlighted a MAGL
50 selectivity greater than 119-fold. Furthermore, very recently Saccomanni and co-workers reported
51 the development of an HPLC/UV assay for the evaluation of MAGL inhibitors.²⁸ Therefore, the
52 activity of compound **17b** against MAGL was also tested by using this method. An aliquot of stock
53
54
55
56
57
58
59
60

1
2
3 solutions of *h*MAGL was diluted 1:125 with Tris buffer (pH = 7.2; 10 mM, containing 1.0 mM
4
5 EDTA) to obtain the working solutions of *h*MAGL at 1.6 ng/ μ l. The stock and working solutions
6
7 were stored at -20° C. In a 0.5 ml spin tube containing 75 μ l of Tris buffer (pH = 7.2; 10 mM
8
9 containing 1.0 mM EDTA), 5 μ l of working solution *h*MAGL (8 ng), and 5 μ l inhibitor (or solvent
10
11 as control) were added. Samples were pre-incubated for 30 min at 37° C and then 5 μ l of a
12
13 solution of 4-NPA in absolute ethanol (4.25 mM) were added. Samples were incubated for 10 min
14
15 at 37° C. The enzymatic reaction was stopped by cooling in an ice bath for 10 min and then 20 μ l
16
17 of the reaction mixture were taken and analyzed by HPLC. Thermo Finnigan HPLC system was
18
19 used to quantify 4-NP formed after enzymatic hydrolysis of 4-NPA by using a UV detector at
20
21 operation wavelength of 315 nm. Separation of compounds was carried out on to reverse-phase
22
23 column (150 mm \times 4.6 mm; 5 μ m). The mobile phase, delivered at a flow rate of 1.0 ml/min and
24
25 consisted of methanol and ammonium acetate buffer (pH 4.0; 10 mM) (53:47, v/v). The sample
26
27 injection volume was 20 μ l. The HPLC system consists of a Thermo Finnigan SpectraSystem
28
29 SN4000 system controller, coupled with P2000 pump, a SCM1000 degasser and a UV2000 UV
30
31 detector at operation wavelength of 315 nm. Data were monitored and analyzed using ChromQuest
32
33 software (Thermo Finnigan, Waltham, MA, USA). Separation of compounds was carried out at r.t.
34
35 on to reverse-phase Chrompack HPLC column SS 150 mm \times 4.6 mm; 5 μ m, with ChromSep guard
36
37 column intersil 5 ODS-3 (Varian, Palo Alto California).
38
39
40
41
42
43

44 By using this assay method, compound **17b** showed an IC_{50} against MAGL of 1.1 ± 0.3 μ M, thus
45
46 confirming the inhibition activity measured by the colorimetric assay.
47
48

49 **General Procedures and Materials.**

50
51
52 All solvents and chemicals were used as purchased without further purification. Chromatographic
53
54 separations were performed on silica gel columns by flash chromatography (Kieselgel 40,
55
56 0.040–0.063 mm; Merck). Reactions were followed by thin layer chromatography (TLC) on Merck
57
58
59
60

1
2
3 aluminum silica gel (60 F254) sheets that were visualized under a UV lamp. Evaporation was
4
5 performed in vacuo (rotating evaporator). Sodium sulfate was always used as the drying agent.
6
7 Proton (^1H) and carbon (^{13}C) NMR spectra were obtained with a Bruker Avance III 400 MHz
8
9 spectrometer using the indicated deuterated solvents. Chemical shifts are given in parts per million
10
11 (ppm) (δ relative to residual solvent peak for ^1H and ^{13}C). ^1H -NMR spectra are reported in this
12
13 order: multiplicity and number of protons. Standard abbreviation indicating the multiplicity were
14
15 used as follows: s = singlet, d = doublet, dd = doublet of doublets, t = triplet, tt = triplet of triplets,
16
17 dt = doublet of triplets, td = triplet of doublets, q = quartet, m = multiplet, bm = broad multiplet and
18
19 bs = broad signal. HPLC analysis: all target compounds (i.e., assessed in biological assays) were \geq
20
21 95% pure by HPLC, confirmed via UV detection ($\lambda = 254$ nm). Analytical reversed-phase HPLC
22
23 was conducted using a Kinetex EVO C18 column (5 μm , 150 \times 4.6 mm, Phenomenex, Inc.); eluent
24
25 A, water; eluent B, CH_3CN ; after 5 min. at 25% B, a gradient was formed from 25% to 75% of B in
26
27 5 min and held at 75% of B for 10 min; flow rate was 1 mL/min. HPLC analyses were performed at
28
29 254 nm, with the exception of compound **8** which was analyzed at 226 nm (UV-visible spectrum
30
31 and superimposition of HPLC chromatograms at 254 e 226 nm of compound **8** are reported in the
32
33 Supporting Information section). Yields refer to isolated and purified products derived from non-
34
35 optimized procedures. Compounds **1** and **2** were purchased from Cayman Chemical and **3** was
36
37 synthesized as previously reported.¹⁶ Compound **4** was characterized as previously reported.¹⁷
38
39
40
41
42

43 **General procedure for the synthesis of benzoylpiperidines 5, 6, 7a-c, 10a-c, 11a-c, 12a-c, 13a-c,**
44 **14a-c, 15b-c, 16a-c, 18c, 19a-c, 20, 30, 31, 44 and benzoylpiperazine 9.** HATU (1.05 equiv) was
45
46 added to a solution of the appropriate benzoic acid (0.447 mmol, 1 equiv) in dry DMF (2.1 mL),
47
48 then DIPEA (0.31 mL, 4 equiv) was added dropwise. The resulting mixture was stirred at room
49
50 temperature for 30 min and then 4-(4-chlorobenzoyl)piperidine **21** (100 mg, 1 equiv) or [1,1'-
51
52 biphenyl]-4-yl(piperidin-4-yl)methanone **38** (for compounds **6** and **44**), or 1-(4-
53
54 chlorobenzoyl)piperazine **41** (for compound **9**) was added and left under stirring at room
55
56
57
58
59
60

1
2
3 temperature until consumption of starting material (TLC). After this time, DMF was evaporated
4
5 under reduced pressure and the residue was diluted with water and extracted with EtOAc. The
6
7 organic layer was washed sequentially with water, saturated brine, dried over Na₂SO₄ and the
8
9 solvent was removed under reduced pressure. The residue was purified with a flash column
10
11 chromatography (silica gel, appropriate mixture of *n*-hexane/ethyl acetate) and pure fractions
12
13 containing the desired compound were evaporated to dryness affording the amides.

14
15 **Synthesis of 4-(4-chlorobenzyl)-1-(4-methoxybenzyl)piperidine (8).** A solution of 4-(4-
16
17 chlorobenzyl)piperidine **39** (0.812 mmol, 1 eq) in 6.8 mL of DMF was treated with K₂CO₃ (3 eq)
18
19 and 4-methoxybenzyl chloride **40** (1.1 eq) and the reaction mixture was stirred at room temperature
20
21 overnight. The mixture was diluted with water and extracted into ethyl acetate. The organic extracts
22
23 were washed successively with water and brine, and the organic solvent was removed under
24
25 vacuum on a rotary evaporator. Crude product was purified by flash chromatography over silica gel.
26
27 Elution with *n*-hexane/EtOAc (6:4) afforded the desired compound as a white solid (yield 53%). ¹H-
28
29 NMR (CDCl₃) δ (ppm): 1.27-1.37 (m, 2H), 1.41-1.52 (m, 1H), 1.54-1.62 (m, 2H), 1.83-1.94 (m,
30
31 2H), 2.49 (d, 2H, *J* = 7.0 Hz), 2.83-2.89 (m, 2H), 3.44 (s, 2H), 3.79 (s, 3H), 6.84 (AA'XX', 2H, *J*_{AX}
32
33 = 8.7 Hz, *J*_{AA'XX'} = 2.5 Hz), 7.04 (AA'XX', 2H, *J*_{AX} = 8.4 Hz, *J*_{AA'XX'} = 2.2 Hz), 7.19-7.24 (m, 4H).
34
35 ¹³C-NMR (CDCl₃) δ (ppm): 32.18 (2C), 38.01, 42.64, 53.71 (2C), 55.38, 62.87, 113.66 (4C),
36
37 128.38, 130.55 (4C), 131.64, 139.33, 158.81. HPLC analysis: retention time = 11.718 min; peak
38
39 area, 99% (226 nm).

40
41 **Procedure for the synthesis of *O*-deprotected benzoylpiperidines 17a-c and 43.** A solution of
42
43 pure amides **4**, **15b-c** or **44** (0.23 mmol) in anhydrous CH₂Cl₂ (2.7 mL) was cooled to -78 °C and
44
45 treated dropwise with a 1.0 M solution of BBr₃ in CH₂Cl₂ (0.73 mL) under argon. The mixture was
46
47 left under stirring at the same temperature for 5 min and then at 0 °C for 1 h and finally at RT until
48
49 starting material was consumed (TLC). The mixture was then diluted with water and extracted with
50
51 ethyl acetate. The organic phase was washed with brine, dried and concentrated. The crude product
52
53
54
55
56
57
58
59
60

1
2
3 was purified by flash chromatography over silica gel. Elution with *n*-hexane/EtOAc (6:4 to 4:6)
4
5 afforded the desired compounds.
6

7 **Procedure of deprotection for the synthesis of compounds 18a-b and 38.** Compounds **30-31** or
8
9 **37** (0.135 mmol) were dissolved in CH₂Cl₂ (0.60 mL), cooled to 0 °C, treated with trifluoroacetic
10
11 acid (0.18 mL) and stirred at rt until consumption of starting material (TLC). The mixture was
12
13 concentrated to dryness under reduced pressure, diluted with EtOAc and washed with 1M solution
14
15 NaHCO₃, then the organic layer was dried over Na₂SO₄ and concentrated. The crude product was
16
17 purified by flash chromatography over silica gel. Elution with *n*-hexane/EtOAc (3:7 to 4:6) or
18
19 CHCl₃/MeOH 85:15 gave the title compounds.
20
21

22 **Procedure for the synthesis of methyl amino-benzoates 24 and 25.** A solution of the appropriate
23
24 commercially available aminobenzoic acids **22** or **23** (1.0 g, 1 equiv) in MeOH (20 mL) was cooled
25
26 to 0 °C followed by a dropwise addition of thionyl chloride (1.3 mL, 2.5 equiv). The mixture was
27
28 refluxed for 3 h. After cooling to rt, evaporation of the solvent and neutralization by addition of a
29
30 saturated aqueous NaHCO₃ solution, the mixture was extracted with EtOAc and the combined
31
32 organic layers were dried over Na₂SO₄ and concentrated. Purification by flash chromatography over
33
34 silica gel and elution with *n*-hexane/EtOAc (7:3) afforded the title compounds.
35
36

37 **Procedure for the synthesis of methyl (*tert*-butoxycarbonyl)amino benzoates 26-27 and *tert*-**
38
39 **butyl 4-(4-chlorobenzoyl)piperidine-1-carboxylate 36.** To a solution of compounds **24-25** or **21**
40
41 (0.1 g, 1 equiv) in dry THF (1.7 mL) and Et₃N (2 equiv), (Boc)₂O (2 equiv for **26** and **27**, 1.2 equiv
42
43 for **36**) was added and the reaction was stirred at room temperature until disappearance of starting
44
45 material (TLC). The solvent was evaporated in vacuo and the residue was dissolved in EtOAc,
46
47 washed with 1M NaHCO₃, water and brine. Then the organic layer was dried over Na₂SO₄ and
48
49 concentrated. The crude product was purified by flash chromatography over silica gel. Elution with
50
51 *n*-hexane/EtOAc (95:5 to 8:2) afforded the desired compounds.
52
53
54

55 **Procedure for the synthesis of (*tert*-butoxycarbonyl)amino benzoic acids 28-29 and [1,1'-**
56
57 **biphenyl]-4-carboxylic acid 35.** Methyl esters **26-27** or **34** (0.1 g) were dissolved in a 1:1 v/v
58
59
60

1
2
3 mixture of THF/methanol (4 mL) and treated with 1.2 mL of 2N aqueous solution of LiOH. The
4
5 reaction was stirred overnight, then the solvents were evaporated, and the residue was treated with 1
6
7 N aqueous HCl and extracted with EtOAc. The organic phase was dried and evaporated to afford
8
9 the pure desired carboxylic acid derivatives.
10

11 **Procedure for the synthesis of methyl 4-bromobenzoate (33).** 4-Bromobenzoic acid **32** (250 mg)
12
13 was dissolved in MeOH until complete dissolution (20 mL), then conc. H₂SO₄ (cat.) was added
14
15 dropwise and the mixture was refluxed overnight. After being cooled to rt, the solvent was
16
17 evaporated in vacuo and the residue was dissolved in EtOAc, washed with 1M NaHCO₃, then the
18
19 organic layer was dried over Na₂SO₄ and concentrated. Pure **33** was obtained as a crystalline light-
20
21 yellow solid (1.13 mmol, 92% yield) and it was used in the next step without any further
22
23 purification.
24
25
26

27 **Procedure for the synthesis of methyl [1,1'-biphenyl]-4-carboxylate (34).** A solution of
28
29 Pd(OAc)₂ (0.03 equiv) and triphenylphosphine (0.15 equiv) in toluene (9.0 mL) was stirred at rt
30
31 under argon for 10 min. After that period, the bromo-aryl precursor **33** (0.93 mmol, 1 equiv),
32
33 K₂CO₃ (1.5 equiv), and phenylboronic acid (2 equiv) were sequentially added. The resulting
34
35 mixture was heated at 100 °C in a sealed vial under argon overnight. After being cooled to rt, the
36
37 mixture was diluted with water and extracted with EtOAc. The combined organic phase was dried
38
39 and concentrated. The crude product was purified by flash chromatography over silica gel. Elution
40
41 with *n*-hexane with 1% EtOAc afforded **34** as a white solid (0.779 mmol, 84% yield).
42
43
44

45 **Procedure for the synthesis of *tert*-butyl 4-([1,1'-biphenyl]-4-carbonyl)piperidine-1-**
46
47 **carboxylate (37).** A solution of **36** (0.182 g, 0.562 mmol, 1 equiv) in anhydrous dioxane (1.7 mL)
48
49 was sequentially treated, under nitrogen, with cesium carbonate (1.7 equiv), phenylboronic acid (1.6
50
51 equiv), Pd₂(dba)₃ (0.032 equiv), and a 20% solution of tricyclohexylphosphine in toluene (0.08
52
53 equiv). The reaction was heated at 100 °C in a sealed vial under argon overnight. The reaction
54
55 mixture was then cooled to rt, diluted with EtOAc, and filtered through a Celite pad. The organic
56
57
58
59
60

1
2
3 filtrate was concentrated under vacuum, and the crude product was purified by flash
4
5 chromatography (*n*-hexane/EtOAc 9:1) to yield pure **37** (0.535 mmol, 95% yield).

6
7 **(1-([1,1'-Biphenyl]-4-carbonyl)piperidin-4-yl)(4-chlorophenyl)methanone (5)**. Yellow solid;
8
9 yield 67% from **21** and **35**; ¹H-NMR (CDCl₃) δ (ppm): 1.78-2.07 (m, 4H), 3.00-3.26 (bm, 2H),
10
11 3.47-3.56 (m, 1H), 3.87-4.07 (bm, 1H), 4.60-4.80 (bm, 1H), 7.38 (tt, 1H, *J* = 7.3, 1.6 Hz), 7.43-7.52
12
13 (m, 6H), 7.57-7.62 (m, 2H), 7.63 (AA'XX', 2H, *J*_{AX} = 8.5 Hz, *J*_{AA'/XX'} = 1.9 Hz), 7.90 (AA'XX', 2H,
14
15 *J*_{AX} = 8.8 Hz, *J*_{AA'/XX'} = 2.2 Hz). ¹³C-NMR (CDCl₃) δ (ppm): 28.73 (2C), 43.46, 127.27 (2C), 127.34
16
17 (2C), 127.61 (2C), 127.91, 129.01 (2C), 129.29 (2C), 129.83 (2C), 134.08, 134.78, 139.90, 140.35,
18
19 142.76, 170.45, 200.53. HPLC analysis: retention time = 13.758 min; peak area, 99% (254 nm).

20
21
22 **(4-([1,1'-Biphenyl]-4-carbonyl)piperidin-1-yl)(4-chlorophenyl)methanone (6)**. Light-yellow
23
24 solid; yield 84% from **38** and 4-chlorobenzoic acid; ¹H-NMR (CDCl₃) δ (ppm): 1.76-2.15 (m, 4H),
25
26 3.00-3.28 (bm, 2H), 3.54-3.63 (m, 1H), 3.76-3.95 (bm, 1H), 4.58-4.78 (bm, 1H), 7.36-7.44 (m, 5H),
27
28 7.45-7.51 (m, 2H), 7.61-7.65 (m, 2H), 7.71 (AA'XX', 2H, *J*_{AX} = 8.6 Hz, *J*_{AA'/XX'} = 1.9 Hz), 8.03
29
30 (AA'XX', 2H, *J*_{AX} = 8.6 Hz, *J*_{AA'/XX'} = 1.9 Hz). ¹³C-NMR (CDCl₃) δ (ppm): 28.75 (2C), 43.44,
31
32 127.37 (3C), 127.59 (2C), 128.48, 128.57 (2C), 128.92 (2C), 129.00 (2C), 129.12, 134.35, 134.42,
33
34 135.87, 139.79, 146.18, 169.52, 201.21. HPLC analysis: retention time = 13.747 min; peak area,
35
36 97% (254 nm).

37
38
39 **Piperidine-1,4-diylbis((4-chlorophenyl)methanone) (7a)**. White solid; yield 60% from **21** and 4-
40
41 chlorobenzoic acid; ¹H-NMR (CDCl₃) δ (ppm): 1.72-2.05 (m, 4H), 3.00-3.20 (bm, 2H), 3.45-3.54
42
43 (m, 1H), 3.72-3.96 (bm, 1H), 4.53-4.72 (bm, 1H), 7.34-7.41 (m, 4H), 7.46 (AA'XX', 2H, *J*_{AX} = 8.8
44
45 Hz, *J*_{AA'/XX'} = 2.2 Hz), 7.89 (AA'XX', 2H, *J*_{AX} = 8.7 Hz, *J*_{AA'/XX'} = 2.2 Hz). ¹³C-NMR (CDCl₃) δ
46
47 (ppm): 28.65 (2C), 43.31, 128.57 (2C), 128.93 (2C), 129.31 (2C), 129.80 (2C), 134.03, 134.37,
48
49 135.93, 139.96, 169.52, 200.40. HPLC analysis: retention time = 13.001 min; peak area, 98% (254
50
51 nm).

52
53
54 **(4-(4-Chlorobenzoyl)piperidin-1-yl)(3-chlorophenyl)methanone (7b)**. Light-yellow solid; yield
55
56 68% from **21** and 3-chlorobenzoic acid; ¹H-NMR (CDCl₃) δ (ppm): 1.73-2.09 (m, 4H), 2.98-3.23
57
58
59
60

(bm, 2H), 3.45-3.55 (m, 1H), 3.74-3.91 (bm, 1H), 4.57-4.73 (bm, 1H), 7.29 (dt, 1H, $J = 7.4, 1.5$ Hz), 7.35 (t, 1H, $J = 8.0$ Hz), 7.38-7.41 (m, 2H), 7.46 (AA'XX', 2H, $J_{AX} = 8.8$ Hz, $J_{AA'/XX'} = 2.2$ Hz), 7.89 (AA'XX', 2H, $J_{AX} = 8.8$ Hz, $J_{AA'/XX'} = 2.2$ Hz). $^{13}\text{C-NMR}$ (CDCl_3) δ (ppm): 28.60 (2C), 43.24, 125.03, 127.15, 129.27 (2C), 129.78 (2C), 129.93, 130.03, 133.97, 134.71, 137.72, 139.91, 168.93, 200.35. HPLC analysis: retention time = 12.961 min; peak area, 99% (254 nm).

(4-(4-Chlorobenzoyl)piperidin-1-yl)(2-chlorophenyl)methanone (7c). Light-yellow solid; yield 58% from **21** and 2-chlorobenzoic acid; $^1\text{H-NMR}$ (CDCl_3) δ (ppm): 1.65-2.04 (m, 4H), 3.02-3.28 (m, 2H), 3.40-3.60 (m, 2H), 4.75 (tt, 1H, $J = 10.9, 4.0$ Hz), 7.30-7.35 (m, 3H), 7.37-7.43 (m, 1H), 7.43-7.48 (m, 2H), 7.86-7.90 (m, 2H). $^{13}\text{C-NMR}$ (CDCl_3 ; asterisk denotes isomer peaks) δ (ppm): 28.41, 28.59, 28.66*, 41.01, 41.16*, 43.18, 43.38*, 45.87, 46.57*, 127.21*, 127.41, 127.67*, 127.84, 129.24*, 129.27, 129.69*, 129.78 (4C), 129.86*, 130.21*, 130.32, 130.37, 130.53*, 134.01, 134.06*, 135.97*, 136.08, 139.80*, 139.90, 166.90*, 167.04, 200.33*, 200.45. HPLC analysis: retention time = 12.699 min; peak area, 99% (254 nm).

(4-(4-Chlorobenzoyl)piperazin-1-yl)(4-methoxyphenyl)methanone (9). White solid; yield 61% from **41** and 4-methoxybenzoic acid **42**; $^1\text{H-NMR}$ (CDCl_3) δ (ppm): 3.43-3.78 (bm, 8H), 3.84 (s, 3H), 6.90-6.95 (m, 2H), 7.34-7.44 (bm, 6H). $^{13}\text{C-NMR}$ (CDCl_3) δ (ppm): 55.52, 114.04 (2C), 126.99, 128.78 (2C), 129.08 (2C), 129.39 (2C), 133.55, 136.42, 161.31, 169.75, 170.87. HPLC analysis: retention time = 10.629 min; peak area, 97% (254 nm).

(4-(4-Chlorobenzoyl)piperidin-1-yl)(4-fluorophenyl)methanone (10a). Light-yellow solid; yield 62% from **21** and 4-fluorobenzoic acid; $^1\text{H-NMR}$ (CDCl_3) δ (ppm): 1.72-2.05 (m, 4H), 3.00-3.20 (bm, 2H), 3.45-3.55 (m, 1H), 3.72-4.00 (bm, 1H), 4.50-4.70 (bm, 1H), 7.10 (double AA'XX', 2H, $^3J_{\text{HF-}o} = 9.5$ Hz, $J_{AX} = 8.7$ Hz, $J_{AA'/XX'} = 2.4$ Hz), 7.40-7.49 (m, 4H), 7.89 (AA'XX', 2H, $J_{AX} = 8.7$ Hz, $J_{AA'/XX'} = 2.2$ Hz). $^{13}\text{C-NMR}$ (CDCl_3) δ (ppm): 28.63 (2C), 43.32, 115.69 (d, 2C, $J = 22.1$ Hz), 129.26 (2C), 129.30 (d, 2C, $J = 9.1$ Hz), 129.78 (2C), 132.00 (d, $J = 3.0$ Hz), 134.00, 139.90, 163.49 (d, $J = 249.5$ Hz), 169.65, 200.41. HPLC analysis: retention time = 12.464 min; peak area, 97% (254 nm).

1
2
3 **(4-(4-Chlorobenzoyl)piperidin-1-yl)(3-fluorophenyl)methanone (10b)**. Light-yellow solid; yield
4 55% from **21** and 3-fluorobenzoic acid; $^1\text{H-NMR}$ (CDCl_3) δ (ppm): 1.73-2.08 (m, 4H), 3.00-3.22
5 (bm, 2H), 3.46-3.54 (m, 1H), 3.75-3.92 (bm, 1H), 4.58-4.74 (bm, 1H), 7.09-7.14 (m, 2H), 7.15 (dt,
6 1H, $J = 7.8, 1.2$ Hz), 7.36-7.42 (m, 1H), 7.46 (AA'XX', 2H, $J_{AX} = 8.8$ Hz, $J_{AA'XX'} = 2.2$ Hz), 7.89
7 (AA'XX', 2H, $J_{AX} = 8.8$ Hz, $J_{AA'XX'} = 2.2$ Hz). $^{13}\text{C-NMR}$ (CDCl_3) δ (ppm): 28.61 (2C), 43.26,
8 114.27 (d, $J = 22.1$ Hz), 116.83, (d, $J = 21.1$ Hz), 122.60 (d, $J = 3.0$ Hz), 129.27 (2C), 129.79 (2C),
9 130.46 (d, $J = 8.0$ Hz), 133.99, 138.06 (d, $J = 7.0$ Hz), 139.91, 162.65 (d, $J = 248.5$ Hz), 169.04,
10 200.37. HPLC analysis: retention time = 12.519 min; peak area, 99% (254 nm).

11 **(4-(4-Chlorobenzoyl)piperidin-1-yl)(2-fluorophenyl)methanone (10c)**. Light-yellow solid; yield
12 64% from **21** and 2-fluorobenzoic acid; $^1\text{H-NMR}$ (CDCl_3) δ (ppm): 1.73-1.87 (m, 3H), 1.98-2.06
13 (m, 1H), 3.02-3.29 (m, 2H), 3.42-3.53 (m, 1H), 3.63-3.72 (m, 1H), 4.68-4.76 (m, 1H), 7.09 (t, 1H, J
14 = 9.6 Hz), 7.21 (td, 1H, $J = 8.0, 0.9$ Hz), 7.36-7.42 (m, 2H), 7.46 (AA'XX', 2H, $J_{AX} = 8.6$ Hz,
15 $J_{AA'XX'} = 2.1$ Hz), 7.89 (AA'XX', 2H, $J_{AX} = 8.7$ Hz, $J_{AA'XX'} = 2.1$ Hz). $^{13}\text{C-NMR}$ (CDCl_3) δ (ppm):
16 28.55, 28.60, 41.43, 43.32, 46.54, 115.89 (d, $J = 21.1$ Hz), 124.32 (d, $J = 18.1$ Hz), 124.83 (d, $J =$
17 3.0 Hz), 129.14 (d, $J = 4.0$ Hz), 129.27 (2C), 129.80 (2C), 131.38 (d, $J = 8.0$ Hz), 134.07, 139.86,
18 158.26 (d, $J = 248.5$ Hz), 165.34, 200.42. HPLC analysis: retention time = 12.439 min; peak area,
19 98% (254 nm).

20 **(1-(4-Bromobenzoyl)piperidin-4-yl)(4-chlorophenyl)methanone (11a)**. Yellow solid; yield 65%
21 from **21** and 4-bromobenzoic acid; $^1\text{H-NMR}$ (CDCl_3) δ (ppm): 1.64-2.00 (m, 4H), 3.04-3.28 (bm,
22 2H), 3.46-3.53 (m, 1H), 3.80-3.90 (bm, 1H), 4.58-4.70 (bm, 1H), 7.30 (AA'XX', 2H, $J_{AX} = 8.4$ Hz,
23 $J_{AA'XX'} = 2.1$ Hz), 7.46 (AA'XX', 2H, $J_{AX} = 8.6$ Hz, $J_{AA'XX'} = 2.2$ Hz), 7.55 (AA'XX', 2H, $J_{AX} = 8.4$
24 Hz, $J_{AA'XX'} = 2.1$ Hz), 7.89 (AA'XX', 2H, $J_{AX} = 8.6$ Hz, $J_{AA'XX'} = 2.1$ Hz). $^{13}\text{C-NMR}$ (CDCl_3) δ
25 (ppm): 28.66 (2C), 43.33, 124.18, 128.78 (2C), 129.33 (2C), 129.83 (2C), 131.92 (2C), 134.02,
26 134.84, 140.00, 169.58, 200.42. HPLC analysis: retention time = 13.127 min; peak area, 98% (254
27 nm).

(1-(3-Bromobenzoyl)piperidin-4-yl)(4-chlorophenyl)methanone (11b). Yellow solid; yield 30% from **21** and 3-bromobenzoic acid; $^1\text{H-NMR}$ (CDCl_3) δ (ppm): 1.74-2.03 (m, 4H), 3.05-3.20 (bm, 2H), 3.47-3.54 (m, 1H), 3.78-3.90 (bm, 1H), 4.64-4.67 (bm, 1H), 7.27-7.35 (m, 2H), 7.47 (AA'XX', 2H, $J_{AX} = 8.6$ Hz, $J_{AA'/XX'} = 2.0$ Hz), 7.55-7.57 (m, 2H), 7.89 (AA'XX', 2H, $J_{AX} = 8.7$ Hz, $J_{AA'/XX'} = 2.1$ Hz). $^{13}\text{C-NMR}$ (CDCl_3) δ (ppm): 28.66 (2C), 43.31, 122.83, 125.54, 129.34 (2C), 129.84 (2C), 130.06, 130.32, 132.93, 134.02, 137.99, 140.00, 168.86, 200.41. HPLC analysis: retention time = 13.126 min; peak area, 97% (254 nm).

(1-(2-Bromobenzoyl)piperidin-4-yl)(4-chlorophenyl)methanone (11c). Orange solid; yield 57% from **21** and 2-bromobenzoic acid; $^1\text{H-NMR}$ (CDCl_3 ; asterisk denotes isomer peaks) δ (ppm): 1.65-2.07 (m, 4H), 3.04-3.15 (m, 1H), 3.20-3.28 (m, 1H), 3.42-3.59 (m, 2H), 4.69-4.80 (m, 1H), 7.22-7.31 (m, 2H), 7.34 (dd, 1H, $J = 7.0, 1.1$ Hz), 7.38* (dd, 1H, $J = 8.3, 1.1$ Hz), 7.44-7.48 (m, 2H), 7.56-7.61 (m, 1H), 7.86-7.90 (m, 2H). $^{13}\text{C-NMR}$ (CDCl_3 ; asterisk denotes isomer peaks) δ (ppm): 28.36*, 28.39, 28.60, 28.65*, 41.01, 41.18*, 43.21, 43.43*, 45.96*, 46.63, 119.21, 119.36*, 127.59*, 127.75, 127.83, 127.97*, 129.28*, 129.31 (2C), 129.81 (2C), 130.34*, 130.45, 132.86*, 133.09, 134.04, 134.09*, 138.18*, 138.31, 139.86, 139.95*, 167.74*, 167.89, 200.36*, 200.48. HPLC analysis: retention time = 12.798 min; peak area, 97% (254 nm).

(4-(4-Chlorobenzoyl)piperidin-1-yl)(4-iodophenyl)methanone (12a). Off-white solid; yield 72% from **21** and 4-iodobenzoic acid; $^1\text{H-NMR}$ (CDCl_3) δ (ppm): 1.71-2.08 (m, 4H), 2.98-3.20 (bm, 2H), 3.44-3.53 (m, 1H), 3.74-3.92 (bm, 1H), 4.57-4.72 (bm, 1H), 7.16 (AA'XX', 2H, $J_{AX} = 8.4$ Hz, $J_{AA'/XX'} = 2.0$ Hz), 7.46 (AA'XX', 2H, $J_{AX} = 8.7$ Hz, $J_{AA'/XX'} = 2.2$ Hz), 7.76 (AA'XX', 2H, $J_{AX} = 8.4$ Hz, $J_{AA'/XX'} = 2.0$ Hz), 7.89 (AA'XX', 2H, $J_{AX} = 8.7$ Hz, $J_{AA'/XX'} = 2.2$ Hz). $^{13}\text{C-NMR}$ (CDCl_3) δ (ppm): 28.61 (2C), 43.26, 95.97, 128.74 (2C), 129.27 (2C), 129.78 (2C), 133.99, 135.39, 137.79 (2C), 139.91, 169.60, 200.36. HPLC analysis: retention time = 13.341 min; peak area, 99% (254 nm).

(4-(4-Chlorobenzoyl)piperidin-1-yl)(3-iodophenyl)methanone (12b). Light-yellow solid; yield 51% from **21** and 3-iodobenzoic acid; $^1\text{H-NMR}$ (CDCl_3) δ (ppm): 1.73-2.08 (m, 4H), 3.00-3.23

(bm, 2H), 3.46-3.55 (m, 1H), 3.75-3.90 (bm, 1H), 4.57-4.73 (bm, 1H), 7.15 (dd, 1H, $J = 8.4, 7.6$ Hz), 7.37 (dt, 1H, $J = 7.9, 1.3$ Hz), 7.47 (AA'XX', 2H, $J_{AX} = 8.8$ Hz, $J_{AA'/XX'} = 2.2$ Hz), 7.74-7.78 (m, 2H), 7.89 (AA'XX', 2H, $J_{AX} = 8.8$ Hz, $J_{AA'/XX'} = 2.2$ Hz). $^{13}\text{C-NMR}$ (CDCl_3) δ (ppm): 28.62 (2C), 43.27, 94.38, 126.05, 129.30 (2C), 129.81 (2C), 130.34, 134.01, 135.79, 138.05, 138.79, 139.94, 168.66, 200.37. HPLC analysis: retention time = 13.301 min; peak area, 98% (254 nm).

(4-(4-Chlorobenzoyl)piperidin-1-yl)(2-iodophenyl)methanone (12c). Yellow solid; yield 57%

from **21** and 2-iodobenzoic acid; $^1\text{H-NMR}$ (CDCl_3 ; asterisk denotes isomer peaks) δ (ppm): 1.65-2.15 (m, 4H), 3.05-3.15 (m, 1H), 3.20-3.30 (m, 1H), 3.45-3.60 (m, 2H), 4.68-4.80 (m, 1H), 7.05-7.11 (m, 1H), 7.18* (dd, 1H, $J = 7.6, 1.6$ Hz), 7.24 (dd, 1H, $J = 7.6, 1.6$ Hz), 7.36-7.43 (m, 1H), 7.44-7.48 (m, 2H), 7.81-7.86 (m, 1H), 7.86-7.91 (m, 2H). $^1\text{H-NMR}$ ($\text{DMSO-}d_6$; asterisk denotes isomer peaks) δ (ppm): 1.38-1.65 (m, 2H), 1.67-1.80 (m, 1H), 1.85-1.96 (m, 1H), 2.93-3.05 (m, 1H), 3.09-3.30 (m, 2H), 3.70-3.82 (m, 1H), 4.47-4.60 (m, 1H), 7.12-7.19 (m, 1H), 7.24* (dd, 1H, $J = 7.4, 1.2$ Hz), 7.29 (dd, 1H, $J = 7.5, 1.3$ Hz), 7.43-7.49 (m, 1H), 7.58-7.64 (m, 2H), 7.85-7.90 (m, 1H), 7.90-8.05 (m, 2H). $^1\text{H-NMR}$ ($\text{DMSO-}d_6$; 80 °C) δ (ppm): 1.50-1.80 (bm, 3H), 1.88-1.99 (bm, 1H), 3.00-3.35 (bm, 3H), 3.68-3.77 (m, 1H), 4.44-4.55 (bm, 1H), 7.15 (td, 1H, $J = 7.7, 1.7$ Hz), 7.23-7.27 (bm, 1H), 7.46 (td, 1H, $J = 7.5, 1.1$ Hz), 7.58 (AA'XX', 2H, $J_{AX} = 8.8$ Hz, $J_{AA'/XX'} = 2.3$ Hz), 7.88 (dd, 1H, $J = 7.9, 0.8$ Hz), 8.00 (AA'XX', 2H, $J_{AX} = 8.7$ Hz, $J_{AA'/XX'} = 2.2$ Hz). $^{13}\text{C-NMR}$ (CDCl_3 ; asterisk denotes isomer peaks) δ (ppm): 28.26*, 28.37, 28.61, 28.66*, 41.06, 41.20*, 43.24, 43.45*, 46.13, 46.71*, 92.44, 92.70*, 126.87*, 127.20, 128.42*, 128.68, 129.30*, 129.33, 129.83 (3C), 130.31*, 130.39, 134.03, 134.08*, 139.25, 139.57*, 139.90*, 139.98, 142.43, 142.56*, 169.42*, 169.52, 200.38*, 200.49. $^{13}\text{C-NMR}$ ($\text{DMSO-}d_6$; asterisk denotes isomer peaks) δ (ppm): 27.77, 27.94*, 28.07*, 28.36, 40.20, 42.24*, 42.38, 45.40*, 45.94, 92.90, 93.17*, 126.79, 126.98*, 128.29, 128.47*, 128.92 (4C), 130.17, 130.21*, 134.01, 138.15, 138.58*, 138.88, 142.30, 142.41*, 167.98, 168.09*, 200.77*, 200.79. $^{13}\text{C-NMR}$ ($\text{DMSO-}d_6$; 80 °C) δ (ppm): 27.36, 27.83, 42.05, 45.30, 92.00, 126.58, 127.94, 128.46 (2C), 129.64 (2C), 129.73, 134.05, 137.73, 138.45, 142.17, 167.75, 200.42. HPLC analysis: retention time = 12.972 min; peak area, 99% (254 nm).

1
2
3 **(4-(4-Chlorobenzoyl)piperidin-1-yl)(*p*-tolyl)methanone (13a)**. Yellow solid; yield 50% from **21**
4 and *p*-toluic acid; ¹H-NMR (CDCl₃) δ (ppm): 1.74-2.00 (m, 4H), 2.38 (s, 3H), 2.95-3.16 (bm, 2H),
5 3.44-3.55 (m, 1H), 3.80-4.15 (bm, 1H), 4.45-4.53 (bm, 1H), 7.19-7.22 (m, 2H), 7.29-7.33 (m, 2H),
6 7.46 (AA'XX', 2H, *J*_{AX} = 8.6 Hz, *J*_{AA'/XX'} = 2.1 Hz), 7.89 (AA'XX', 2H, *J*_{AX} = 8.6 Hz, *J*_{AA'/XX'} = 2.1
7 Hz). ¹³C-NMR (CDCl₃) δ (ppm): 21.49, 28.71 (2C), 43.49, 127.13 (2C), 129.21 (2C), 129.26 (2C),
8 129.82 (2C), 133.05, 134.10, 139.85, 139.96, 170.80, 200.56. HPLC analysis: retention time =
9 12.754 min; peak area, 97% (254 nm).
10
11

12 **(4-(4-Chlorobenzoyl)piperidin-1-yl)(*m*-tolyl)methanone (13b)**. Orange solid; yield 51% from **21**
13 and *m*-toluic acid; ¹H-NMR (CDCl₃) δ (ppm): 1.74-2.00 (m, 4H), 2.37 (s, 3H), 3.00-3.18 (bm, 2H),
14 3.45-3.53 (m, 1H), 3.80-4.00 (bm, 1H), 4.55-4.80 (bm, 1H), 7.77-7.24 (m, 3H), 7.28 (t, 1H, *J* = 7.8
15 Hz), 7.46 (AA'XX', 2H, *J*_{AX} = 8.7 Hz, *J*_{AA'/XX'} = 2.2 Hz), 7.89 (AA'XX', 2H, *J*_{AX} = 8.7 Hz, *J*_{AA'/XX'} =
16 2.2 Hz). ¹³C-NMR (CDCl₃) δ (ppm): 21.47, 28.70 (2C), 43.47, 123.85, 127.55, 128.43 (2C), 129.26
17 (2C), 129.80, 130.48, 134.08, 136.02, 138.53, 139.86, 170.77, 200.54. HPLC analysis: retention
18 time = 12.766 min; peak area, 96% (254 nm).
19
20

21 **(4-(4-Chlorobenzoyl)piperidin-1-yl)(*o*-tolyl)methanone (13c)**. Orange solid; yield 46% from **21**
22 and *o*-toluic acid; ¹H-NMR (CDCl₃; asterisk denotes isomer peaks) δ (ppm): 1.68-1.85 (m, 3H),
23 1.98-2.08 (m, 1H), 2.30* (s, 3H), 2.34 (s, 3H), 2.97-3.16 (m, 2H), 3.42-3.55 (m, 1H), 3.56-3.65 (m,
24 1H), 4.70-4.83 (m, 1H), 7.11-7.30 (m, 4H), 7.46 (AA'XX', 2H, *J*_{AX} = 8.8 Hz, *J*_{AA'/XX'} = 2.2 Hz),
25 7.88 (AA'XX', 2H, *J*_{AX} = 8.8 Hz, *J*_{AA'/XX'} = 2.0 Hz). ¹³C-NMR (CDCl₃; asterisk denotes isomer
26 peaks) δ (ppm): 19.10, 19.21*, 28.55*, 28.81, 28.95*, 40.98, 43.30*, 43.53, 46.11*, 46.48, 125.81,
27 125.96*, 126.16, 128.99, 129.29 (2C), 129.79 (2C), 130.49, 130.66*, 134.05, 134.10, 134.41*,
28 136.32, 139.92, 170.07*, 179.17, 200.46, 200.56*. HPLC analysis: retention time = 12.588 min;
29 peak area, 97% (254 nm).
30
31

32 **(4-(4-Chlorobenzoyl)piperidin-1-yl)(4-(trifluoromethyl)phenyl)methanone (14a)**. Orange solid;
33 yield 54% from **21** and 4-(trifluoromethyl)benzoic acid; ¹H-NMR (CDCl₃) δ (ppm): 1.73-2.10 (m,
34 4H), 3.02-3.24 (bm, 2H), 3.48-3.56 (m, 1H), 3.71-3.83 (bm, 1H), 4.61-4.75 (bm, 1H), 7.47
35
36
37
38
39
40
41
42
43
44
45
46
47
48
49
50
51
52
53
54
55
56
57
58
59
60

(AA'XX', 2H, $J_{AX} = 8.8$ Hz, $J_{AA'XX'} = 2.2$ Hz), 7.51-7.55 (m, 2H), 7.67-7.71 (m, 2H), 7.89 (AA'XX', 2H, $J_{AX} = 8.7$ Hz, $J_{AA'XX'} = 2.2$ Hz). $^{13}\text{C-NMR}$ (CDCl_3) δ (ppm): 28.64 (2C), 43.22, 123.84 (q, $J = 272.7$ Hz), 125.79 (q, 2C, $J = 4.0$ Hz), 127.37, 129.33 (2C), 129.82 (2C), 131.81 (q, $J = 32.2$ Hz), 133.99, 139.63 (q, 2C, $J = 1.0$ Hz), 140.02, 169.08, 200.33. HPLC analysis: retention time = 13.273 min; peak area, 96% (254 nm).

(4-(4-Chlorobenzoyl)piperidin-1-yl)(3-(trifluoromethyl)phenyl)methanone (14b). Orange solid; yield 41% from **21** and 3-(trifluoromethyl)benzoic acid; $^1\text{H-NMR}$ (CDCl_3) δ (ppm): 1.74-2.09 (m, 4H), 3.02-3.28 (bm, 2H), 3.46-3.57 (m, 1H), 3.70-3.88 (bm, 1H), 4.58-4.76 (bm, 1H), 7.47 (AA'XX', 2H, $J_{AX} = 8.7$ Hz, $J_{AA'XX'} = 2.2$ Hz), 7.55 (t, 1H, $J = 8.3$ Hz), 7.59-7.63 (m, 1H), 7.67-7.71 (m, 2H), 7.89 (AA'XX', 2H, $J_{AX} = 8.7$ Hz, $J_{AA'XX'} = 2.2$ Hz). $^{13}\text{C-NMR}$ (CDCl_3) δ (ppm): 28.59 (2C), 43.19, 123.77 (q, $J = 273.7$ Hz), 124.04, 126.59, 129.29 (3C), 129.80 (2C), 130.30, 131.24 (q, $J = 33.2$ Hz), 133.98, 136.82, 139.97, 168.95, 200.31. HPLC analysis: retention time = 13.234 min; peak area, 98% (254 nm).

(4-(4-Chlorobenzoyl)piperidin-1-yl)(2-(trifluoromethyl)phenyl)methanone (14c). Orange solid; yield 55% from **21** and 2-(trifluoromethyl)benzoic acid; $^1\text{H-NMR}$ (CDCl_3 ; asterisk denotes isomer peaks) δ (ppm): 1.65-1.84 (m, 2H), 1.97-2.08 (m, 2H), 3.03-3.18 (m, 2H), 3.40-3.53 (m, 2H), 4.68-4.77 (m, 1H), 7.32* (d, 1H, $J = 7.8$ Hz), 7.37 (d, 1H, $J = 7.6$ Hz), 7.43-7.48 (m, 2H), 7.49-7.55 (m, 1H), 7.57-7.63 (m, 1H), 7.69-7.73 (m, 1H), 7.85-7.90 (m, 2H). $^{13}\text{C-NMR}$ (CDCl_3 ; asterisk denotes isomer peaks) δ (ppm): 27.77*, 28.16, 28.23*, 28.62, 41.10, 41.16*, 43.17, 43.20*, 46.60, 46.63*, 123.77* (q, $J = 274.2$ Hz), 123.80 (q, $J = 273.7$ Hz), 126.71 (q, $J = 4.7$ Hz), 126.73 (q, $J = 31.9$ Hz), 126.94* (q, $J = 5.0$ Hz), 127.22*, 127.25, 128.56, 128.93*, 129.26 (2C), 129.31* (2C), 129.79* (2C), 129.81 (2C), 132.20*, 132.44, 133.98, 134.05*, 135.01* (q, $J = 2.0$ Hz), 135.10 (q, $J = 2.0$ Hz), 139.83*, 139.98, 167.41*, 167.56, 200.20*, 200.48. HPLC analysis: retention time = 13.008 min; peak area, 96% (254 nm).

(4-(4-Chlorobenzoyl)piperidin-1-yl)(3-methoxyphenyl)methanone (15b). White solid; yield 67% from **21** and 3-methoxybenzoic acid; $^1\text{H-NMR}$ (CDCl_3) δ (ppm): 1.72-2.02 (m, 4H), 3.00-3.20 (bm,

1
2
3 2H), 3.45-3.53 (m, 1H), 3.82 (s, 3H), 3.80-3.95 (bm, 1H), 4.60-4.75 (bm, 1H), 6.93-6.98 (m, 3H),
4
5 7.28-7.33 (m, 1H), 7.46 (AA'XX', 2H, $J_{AX} = 8.8$ Hz, $J_{AA'/XX'} = 2.2$ Hz), 7.89 (AA'XX', 2H, $J_{AX} =$
6
7 8.8 Hz, $J_{AA'/XX'} = 2.2$ Hz). ^{13}C -NMR (CDCl_3) δ (ppm): 28.71 (2C), 43.46, 55.50, 112.32, 115.73,
8
9 119.01, 129.30 (2C), 129.76, 129.82 (2C), 134.11, 137.36, 139.91, 159.83, 170.34, 200.53. HPLC
10
11 analysis: retention time = 12.387 min; peak area, 97% (254 nm).

12
13 **(4-(4-Chlorobenzoyl)piperidin-1-yl)(2-methoxyphenyl)methanone (15c)**. Orange solid; yield
14
15 36% from **21** and 2-methoxybenzoic acid; ^1H -NMR (CDCl_3 ; asterisk denotes isomer peaks) δ
16
17 (ppm): 1.70-2.05 (m, 4H), 2.97-3.20 (m, 2H), 3.40-3.50 (m, 1H), 3.57-3.65 (m, 1H), 3.84* (s, 3H),
18
19 3.85 (s, 3H), 4.72-4.81 (m, 1H), 6.89-6.93 (m, 1H), 6.96-7.02 (m, 1H), 7.21-7.25 (m, 1H), 7.32-7.37
20
21 (m, 1H), 7.43-7.48 (m, 2H), 7.86-7.91 (m, 2H). ^{13}C -NMR (CDCl_3 ; asterisk denotes isomer peaks) δ
22
23 (ppm): 28.63, 28.70*, 41.13*, 41.23, 43.55, 43.63*, 46.12*, 46.74, 55.66, 55.74*, 110.99*, 111.08,
24
25 121.01*, 121.15, 125.92, 126.03*, 127.94, 128.05*, 129.26 (2C), 129.81 (2C), 130.50*, 130.54,
26
27 134.17, 139.82, 139.84*, 155.44*, 155.51, 167.87*, 168.09, 200.61, 200.70*. HPLC analysis:
28
29 retention time = 12.219 min; peak area, 95% (254 nm).

30
31
32
33 **(4-(4-Chlorobenzoyl)piperidin-1-yl)(4-(trifluoromethoxy)phenyl)methanone (16a)**. Orange
34
35 solid; yield 54% from **21** and 4-(trifluoromethoxy)benzoic acid; ^1H -NMR (CDCl_3) δ (ppm): 1.74-
36
37 2.07 (m, 4H), 3.01-3.23 (bm, 2H), 3.46-3.55 (m, 1H), 3.74-3.95 (bm, 1H), 4.53-4.76 (bm, 1H),
38
39 7.24-7.28 (m, 2H), 7.44-7.49 (m, 4H), 7.89 (AA'XX', 2H, $J_{AX} = 8.7$ Hz, $J_{AA'/XX'} = 2.0$ Hz). ^{13}C -
40
41 NMR (CDCl_3) δ (ppm): 28.65 (2C), 43.28, 120.49 (q, $J = 258.2$ Hz), 121.06 (2C), 128.87 (2C),
42
43 129.31 (2C), 129.81 (2C), 134.03, 134.60, 139.97, 150.17 (q, $J = 1.3$ Hz), 169.28, 200.38. HPLC
44
45 analysis: retention time = 13.405 min; peak area, 98% (254 nm).

46
47
48
49 **(4-(4-Chlorobenzoyl)piperidin-1-yl)(3-(trifluoromethoxy)phenyl)methanone (16b)**. Orange
50
51 solid; yield 47% from **21** and 3-(trifluoromethoxy)benzoic acid; ^1H -NMR (CDCl_3) δ (ppm): 1.74-
52
53 2.10 (m, 4H), 3.00-3.25 (bm, 2H), 3.45-3.55 (m, 1H), 3.72-3.90 (bm, 1H), 4.58-4.73 (bm, 1H),
54
55 7.25-7.30 (m, 2H), 7.35 (d, 1H, $J = 7.6$ Hz), 7.43-7.49 (m, 3H), 7.87-7.91 (m, 2H). ^{13}C -NMR
56
57 (CDCl_3) δ (ppm): 28.60 (2C), 43.25, 119.73, 120.52 (q, $J = 257.9$ Hz), 122.24, 125.37, 129.31 (2C),
58
59
60

1
2
3 129.81 (2C), 130.34, 134.03, 137.94, 139.98, 149.32 (q, $J = 2.0$ Hz), 168.78, 200.34. HPLC
4
5 analysis: retention time = 13.420 min; peak area, 97% (254 nm).
6

7 **(4-(4-Chlorobenzoyl)piperidin-1-yl)(2-(trifluoromethoxy)phenyl)methanone (16c)**. Orange
8
9 solid; yield 50% from **21** and 2-(trifluoromethoxy)benzoic acid; $^1\text{H-NMR}$ (CDCl_3) δ (ppm): 1.70-
10 2.04 (m, 4H), 3.02-3.26 (m, 2H), 3.40-3.62 (m, 2H), 4.68-4.78 (m, 1H), 7.28-7.48 (m, 6H), 7.89
11
12 (AA'XX', 2H, $J_{AX} = 8.6$ Hz, $J_{AA'/XX'} = 2.1$ Hz). $^{13}\text{C-NMR}$ (CDCl_3 ; asterisk denotes isomer peaks) δ
13 (ppm): 28.36*, 28.46, 28.52*, 28.63, 41.19, 41.39*, 43.17, 43.35*, 46.17, 46.68*, 120.55 (q, $J =$
14 258.6 Hz), 120.61, 120.68*, 127.30*, 127.38, 128.75, 128.85*, 129.30, 129.81 (4C), 130.80, 134.02,
15 134.07*, 139.83*, 139.97, 145.00, 165.62, 200.22*, 200.47. HPLC analysis: retention time =
16 13.205 min; peak area, 97% (254 nm).
17
18
19
20
21
22
23

24 **(4-(4-Chlorobenzoyl)piperidin-1-yl)(4-hydroxyphenyl)methanone (17a)**. Beige solid; yield 69%
25 from **4**; $^1\text{H-NMR}$ ($\text{DMSO-}d_6$) δ (ppm): 1.43-1.55 (m, 2H), 1.76-1.87 (m, 2H), 2.99-3.16 (bm, 2H),
26 3.73 (tt, 1H, $J = 11.1, 3.5$ Hz), 3.95-4.30 (bm, 2H), 6.77 (AA'XX', 2H, $J_{AX} = 8.7$ Hz, $J_{AA'/XX'} = 2.4$
27 Hz), 7.25 (AA'XX', 2H, $J_{AX} = 8.7$ Hz, $J_{AA'/XX'} = 2.4$ Hz), 7.61 (AA'XX', 2H, $J_{AX} = 8.8$ Hz, $J_{AA'/XX'} =$
28 2.2 Hz), 8.02 (AA'XX', 2H, $J_{AX} = 8.8$ Hz, $J_{AA'/XX'} = 2.3$ Hz), 9.82 (exchangeable bs, 1H). $^{13}\text{C-NMR}$
29 (DMSO- d_6) δ (ppm): 28.29 (2C), 42.49, 114.85 (2C), 126.37, 128.94 (2C), 128.95 (2C), 130.18
30 (2C), 134.12, 138.13, 158.58, 169.33, 200.93. HPLC analysis: retention time = 11.077 min; peak
31 area, 99% (254 nm).
32
33
34
35
36
37
38
39
40
41
42

43 **(4-(4-Chlorobenzoyl)piperidin-1-yl)(3-hydroxyphenyl)methanone (17b)**. White solid; yield 94%
44 from **15b**; $^1\text{H-NMR}$ (acetone- d_6) δ (ppm): 1.59-1.71 (m, 2H), 1.81-2.00 (bm, 2H), 2.90-3.30 (bm,
45 2H), 3.79 (tt, 1H, $J = 11.3, 3.7$ Hz), 4.40-4.70 (bm, 2H), 6.85-6.92 (m, 3H), 7.23-7.28 (m, 1H), 7.57
46 (AA'XX', 2H, $J_{AX} = 8.8$ Hz, $J_{AA'/XX'} = 2.2$ Hz), 8.07 (AA'XX', 2H, $J_{AX} = 8.8$ Hz, $J_{AA'/XX'} = 2.3$ Hz),
47 8.58 (exchangeable bs, 1H). $^{13}\text{C-NMR}$ (acetone- d_6) δ (ppm): 44.02, 114.62, 117.12, 118.71, 129.83
48 (2C), 130.40, 131.00 (2C), 135.55, 139.11, 139.59, 158.27, 170.14, 201.33. HPLC analysis:
49 retention time = 11.262 min; peak area, 99% (254 nm).
50
51
52
53
54
55
56
57
58
59
60

(4-(4-Chlorobenzoyl)piperidin-1-yl)(2-hydroxyphenyl)methanone (17c). Grey solid; yield 76% from **15c**; $^1\text{H-NMR}$ (acetone- d_6) δ (ppm): 1.66-1.78 (m, 2H), 1.92-2.00 (m, 2H), 3.17-3.28 (m, 2H), 3.81 (tt, 1H, $J = 11.2, 3.7$ Hz), 4.22-4.35 (bm, 2H), 6.87-6.95 (m, 2H), 7.27-7.32 (m, 2H), 7.57 (AA'XX', 2H, $J_{AX} = 8.7$ Hz, $J_{AA'/XX'} = 2.2$ Hz), 8.07 (AA'XX', 2H, $J_{AX} = 8.7$ Hz, $J_{AA'/XX'} = 2.2$ Hz), 9.33 (exchangeable s, 1H). $^{13}\text{C-NMR}$ (acetone- d_6) δ (ppm): 43.95, 117.48, 119.93, 122.03, 129.35, 129.84 (2C), 131.01, 132.10 (2C), 135.56, 139.60, 157.19, 169.72, 201.31. HPLC analysis: retention time = 11.492 min; peak area, 99% (254 nm).

(1-(4-Aminobenzoyl)piperidin-4-yl)(4-chlorophenyl)methanone (18a). Beige solid; yield 77% from **31**; $^1\text{H-NMR}$ (acetone- d_6) δ (ppm): 1.58-1.70 (m, 2H), 1.86-1.94 (m, 2H), 3.06-3.16 (m, 2H), 3.76 (tt, 1H, $J = 11.3, 3.8$ Hz), 4.22-4.32 (bm, 1H), 4.93-5.03 (bm, 1H), 6.67 (AA'XX', 2H, $J_{AX} = 8.6$ Hz, $J_{AA'/XX'} = 2.3$ Hz), 7.21 (AA'XX', 2H, $J_{AX} = 8.6$ Hz, $J_{AA'/XX'} = 2.2$ Hz), 7.57 (AA'XX', 2H, $J_{AX} = 8.8$ Hz, $J_{AA'/XX'} = 2.3$ Hz), 8.06 (AA'XX', 2H, $J_{AX} = 8.8$ Hz, $J_{AA'/XX'} = 2.2$ Hz). $^{13}\text{C-NMR}$ (acetone- d_6) δ (ppm): 44.17, 114.00 (2C), 119.92, 129.02, 129.79 (2C), 130.03 (2C), 130.98 (2C), 135.55, 139.51, 171.15, 201.40. HPLC analysis: retention time = 11.037 min; peak area, 98% (254 nm).

(1-(3-Aminobenzoyl)piperidin-4-yl)(4-chlorophenyl)methanone (18b). Beige solid; yield 89% from **30**; $^1\text{H-NMR}$ (acetone- d_6) δ (ppm): 1.57-1.68 (m, 2H), 1.83-1.95 (bm, 2H), 2.90-3.30 (bm, 2H), 3.78 (tt, 1H, $J = 11.2, 3.7$ Hz), 4.76-4.82 (bm, 2H), 6.60 (dt, 1H, $J = 7.5, 1.3$ Hz), 6.69-6.73 (m, 2H), 7.09 (dd, 1H, $J = 8.7, 7.5$ Hz), 7.57 (AA'XX', 2H, $J_{AX} = 8.8$ Hz, $J_{AA'/XX'} = 2.3$ Hz), 8.06 (AA'XX', 2H, $J_{AX} = 8.8$ Hz, $J_{AA'/XX'} = 2.2$ Hz). $^{13}\text{C-NMR}$ (acetone- d_6) δ (ppm): 44.08, 113.35, 115.69, 115.86, 129.77, 129.82 (2C), 130.99 (2C), 135.55, 138.56, 139.57, 149.44, 170.83, 201.37. HPLC analysis: retention time = 11.188 min; peak area, 99% (254 nm).

(1-(2-Aminobenzoyl)piperidin-4-yl)(4-chlorophenyl)methanone (18c). Orange solid; yield 44% from **21** and anthranilic acid; $^1\text{H-NMR}$ (acetone- d_6) δ (ppm): 1.62-1.73 (m, 2H), 1.88-1.97 (m, 2H), 3.10-3.21 (m, 2H), 3.78 (tt, 1H, $J = 11.3, 3.7$ Hz), 4.14-4.32 (bm, 1H), 4.87-4.95 (bm, 1H), 6.62 (td, 1H, $J = 7.4, 1.0$ Hz), 6.78 (dd, 1H, $J = 8.1, 0.7$ Hz), 7.07-7.14 (m, 2H), 7.57 (AA'XX', 2H, $J_{AX} =$

8.8 Hz, $J_{AA'XX'}$ = 2.2 Hz), 8.06 (AA'XX', 2H, J_{AX} = 8.8 Hz, $J_{AA'XX'}$ = 2.3 Hz). $^{13}\text{C-NMR}$ (acetone- d_6) δ (ppm): 44.06, 116.84, 116.94, 120.83, 128.61, 129.79, 129.80 (2C), 130.98 (2C), 135.53, 139.54, 147.44, 170.21, 201.32. HPLC analysis: retention time = 11.795 min; peak area, 95% (254 nm).

(4-(4-Chlorobenzoyl)piperidin-1-yl)(4-nitrophenyl)methanone (19a). Yellow solid; yield 48% from **21** and 4-nitrobenzoic acid; $^1\text{H-NMR}$ (CDCl_3) δ (ppm): 1.74-2.10 (m, 4H), 3.04-3.28 (bm, 2H), 3.49-3.59 (m, 1H), 3.66-3.80 (bm, 1H), 4.61-4.73 (bm, 1H), 7.47 (AA'XX', 2H, J_{AX} = 8.8 Hz, $J_{AA'XX'}$ = 2.2 Hz), 7.59 (AA'XX', 2H, J_{AX} = 8.9 Hz, $J_{AA'XX'}$ = 2.1 Hz), 7.89 (AA'XX', 2H, J_{AX} = 8.8 Hz, $J_{AA'XX'}$ = 2.2 Hz), 8.29 (AA'XX', 2H, J_{AX} = 8.8 Hz, $J_{AA'XX'}$ = 2.1 Hz). $^{13}\text{C-NMR}$ (CDCl_3) δ (ppm): 28.61 (2C), 43.10, 124.05 (2C), 128.05 (2C), 129.35 (2C), 129.80 (2C), 134.07, 140.08, 142.25, 148.65, 168.19, 200.16. HPLC analysis: retention time = 12.470 min; peak area, 99% (254 nm).

(4-(4-Chlorobenzoyl)piperidin-1-yl)(3-nitrophenyl)methanone (19b). Orange solid; yield 55% from **21** and 3-nitrobenzoic acid; $^1\text{H-NMR}$ (CDCl_3) δ (ppm): 1.77-2.10 (m, 4H), 3.08-3.30 (bm, 2H), 3.49-3.58 (m, 1H), 3.72-3.85 (bm, 1H), 4.58-4.73 (bm, 1H), 7.47 (AA'XX', 2H, J_{AX} = 8.7 Hz, $J_{AA'XX'}$ = 2.2 Hz), 7.63 (td, 1H, J = 7.6, 1.3 Hz), 7.77 (dt, 1H, J = 7.7, 1.3 Hz), 7.89 (AA'XX', 2H, J_{AX} = 8.7 Hz, $J_{AA'XX'}$ = 2.2 Hz), 8.27-8.31 (m, 2H). $^{13}\text{C-NMR}$ (CDCl_3) δ (ppm): 28.55 (2C), 43.03, 122.22, 124.62, 129.31 (2C), 129.79 (2C), 129.96, 133.03, 133.94, 137.60, 139.99, 148.21, 167.84, 200.20. HPLC analysis: retention time = 12.445 min; peak area, 96% (254 nm).

(4-(4-Chlorobenzoyl)piperidin-1-yl)(2-nitrophenyl)methanone (19c). Light-yellow solid; yield 54% from **21** and 2-nitrobenzoic acid; $^1\text{H-NMR}$ (CDCl_3) δ (ppm): 1.71-1.86 (bm, 3H), 2.02-2.13 (bm, 1H), 3.10-3.25 (bm, 2H), 3.42-3.56 (bm, 2H), 4.57-4.76 (bm, 1H), 7.36-7.48 (m, 3H), 7.57 (td, 1H, J = 8.5, 1.3 Hz), 7.68-7.75 (m, 1H), 7.84-7.91 (m, 2H), 8.20 (d, 1H, J = 8.2 Hz). $^{13}\text{C-NMR}$ (CDCl_3) δ (ppm): 27.96, 28.38, 41.27, 43.01, 46.01, 124.95, 128.12, 129.33, 129.83 (3C), 129.96, 133.16, 134.05, 134.78, 140.00, 145.30, 166.90, 200.58. HPLC analysis: retention time = 12.240 min; peak area, 97% (254 nm).

1
2
3 **(1-Benzoylpiperidin-4-yl)(4-chlorophenyl)methanone (20)**. Light-yellow solid; yield 61% from
4 **21** and benzoic acid; $^1\text{H-NMR}$ (CDCl_3) δ (ppm): 1.70-2.00 (m, 4H), 2.97-3.23 (bm, 2H), 3.45-3.53
5 (m, 1H), 3.80-3.95 (bm, 1H), 4.57-4.70 (bm, 1H), 7.41 (s, 5H), 7.46 (AA'XX', 2H, $J_{AX} = 8.6$ Hz,
6 $J_{AA'XX'} = 2.1$ Hz), 7.89 (AA'XX', 2H, $J_{AX} = 8.6$ Hz, $J_{AA'XX'} = 2.1$ Hz). $^{13}\text{C-NMR}$ (CDCl_3) δ (ppm):
7 28.71 (2C), 43.47, 127.00 (2C), 128.64 (2C), 129.30, 129.82 (4C), 134.11, 136.09, 139.92, 170.62,
8 200.52. HPLC analysis: retention time = 12.259 min; peak area, 98% (254 nm).

9
10
11
12
13
14
15 **(4-([1,1'-Biphenyl]-4-carbonyl)piperidin-1-yl)(3-hydroxyphenyl)methanone (43)**. White solid;
16 yield 82% from **44**; $^1\text{H-NMR}$ ($\text{DMSO-}d_6$) δ (ppm): 1.46-1.59 (m, 2H), 1.72-1.98 (bm, 2H), 2.90-
17 3.10 (bm, 1H), 3.10-3.30 (bm, 1H), 3.60-3.75 (bm, 1H), 3.80 (tt, 1H, $J = 11.2, 3.4$ Hz), 4.40-4.57
18 (bm, 1H), 6.74-6.80 (m, 2H), 6.82 (ddd, 1H, $J = 8.1, 2.5, 1.0$ Hz), 7.23 (t, 1H, $J = 7.7$ Hz), 7.44 (tt,
19 1H, $J = 7.3, 1.5$ Hz), 7.48-7.54 (m, 2H), 7.73-7.78 (m, 2H), 7.82-7.87 (m, 2H), 8.08-8.12 (m, 2H),
20 9.67 (exchangeable s, 1H). 9.82 (exchangeable bs, 1H). $^{13}\text{C-NMR}$ ($\text{DMSO-}d_6$) δ (ppm): 42.43,
21 113.40, 116.31, 117.09, 127.03 (2C), 127.07 (2C), 128.44, 129.04 (2C), 129.12 (2C), 129.62,
22 134.24, 137.51, 138.88, 144.66, 157.29, 168.95, 201.46. HPLC analysis: retention time = 12.153
23 min; peak area, 99% (254 nm).

24
25
26
27
28
29
30
31
32
33
34
35
36 **Docking Calculations.** The crystal structure of *hMAGL* (pdb code 3PE6²⁰) was taken from the
37 Protein Data Bank.²⁹ After adding hydrogen atoms the protein complexed with its reference
38 inhibitor was minimized using Amber14 software³⁰ and ff14SB force field at 300 K. The complex
39 was placed in a rectangular parallelepiped water box, an explicit solvent model for water, TIP3P,
40 was used and the complex was solvated with a 10 Å water cap. Sodium ions were added as counter
41 ions to neutralize the system. Two steps of minimization were then carried out; in the first stage, we
42 kept the protein fixed with a position restraint of 500 kcal/mol Å² and we solely minimized the
43 positions of the water molecules. In the second stage, we minimized the entire system through 5000
44 steps of steepest descent followed by conjugate gradient (CG) until a convergence of 0.05
45 kcal/Å•mol. The ligands were built using Maestro³¹ and were minimized by means of
46 Macromodel³² in a water environment using the CG method until a convergence value of 0.05
47
48
49
50
51
52
53
54
55
56
57
58
59
60

1
2
3 kcal/Å mol, using the MMFFs force field and a distance-dependent dielectric constant of 1.0.
4 Automated docking was carried out by means of the AUTODOCK 4.0 program;³³ Autodock
5 Tools³⁴ was used in order to identify the torsion angles in the ligands, add the solvent model and
6
7 assign the Kollman atomic charges to the protein. The ligand charge was calculated using the
8
9 Gasteiger method. The regions of interest used by Autodock were defined by considering the ZYH
10
11 reference inhibitor as the central group; in particular, a grid of 82, 40, and 30 points in the x, y, and
12
13 z directions was constructed centered on the center of the mass of this compound. A grid spacing of
14
15 0.375 Å and a distance-dependent function of the dielectric constant were used for the energetic
16
17 map calculations. Using the Lamarckian Genetic Algorithm, the docked compounds were subjected
18
19 to 100 runs of the Autodock search, using 500000 steps of energy evaluation and the default values
20
21 of the other parameters. Cluster analysis was performed on the results using an RMS tolerance of
22
23 2.0 Å.
24
25
26
27
28

29 **MD Simulations.** All simulations were performed using AMBER, version 14.³⁰ MD simulations
30
31 were carried out using the ff14SB force field at 300 K. The complex was placed in a rectangular
32
33 parallelepiped water box. An explicit solvent model for water, TIP3P, was used, and the complex
34
35 was solvated with a 20 Å water cap. Sodium ions were added as counterions to neutralize the
36
37 system. Prior to MD simulations, two steps of minimization were carried out using the same
38
39 procedure described above. Particle Mesh Ewald (PME) electrostatics and periodic boundary
40
41 conditions were used in the simulation.³⁵ The MD trajectory was run using the minimized structure
42
43 as the starting conformation. The time step of the simulations was 2.0 fs with a cutoff of 10 Å for
44
45 the nonbonded interaction, and SHAKE was employed to keep all bonds involving hydrogen atoms
46
47 rigid. Constant-volume periodic boundary MD was carried out for 1.0 ns, during which the
48
49 temperature was raised from 0 to 300 K. Then 50 ns of constant pressure periodic boundary MD
50
51 was carried out at 300 K using the Langevin thermostat to maintain constant the temperature of our
52
53 system. All the α carbons of the protein were blocked with a harmonic force constant of 10
54
55 kcal/mol•Å². General Amber force field (GAFF) parameters were assigned to the ligand, while
56
57
58
59
60

1
2
3 partial charges were calculated using the AM1-BCC method as implemented in the Antechamber
4 suite of AMBER 14. The final structure of the complex was obtained as the average of the last 50.0
5 ns of MD minimized by the CG method until a convergence of 0.05 kcal/mol·Å². The average
6 structure was obtained using the Cpptraj program³⁶ implemented in AMBER 14.

7
8
9
10
11 **MAGL inhibition assay.** Human recombinant MAGL, **1**, **2** and 4-NPA substrate were from
12 Cayman Chemical. The IC₅₀ values for compounds were generated in 96-well microtiter plates. The
13 MAGL reaction was conducted at room temperature at a final volume of 200 μL in 10 mM Tris
14 buffer, pH 7.2, containing 1 mM EDTA and BSA 0.1 mg/ml. A total of 150 μL of 4-NPA 133.3 μM
15 was added to 10 μL of DMSO containing the appropriate amount of compound. The reaction was
16 initiated by the addition of 40 μL of MAGL (11 ng/well) in such a way that the assay was linear
17 over 30 min. The final concentration of the analyzed compounds ranged for **1** and **2** from 10 to
18 0.00001 μM and for the other compounds from 200 to 0.0128 μM. After the reaction had proceeded
19 for 30 min, absorbance values were then measured by using a Victor X3 Microplates Reader
20 (PerkinElmer®) at 405 nm.⁵ Two reactions were also run: one reaction containing no compounds
21 and the second one containing neither inhibitor nor enzyme. IC₅₀ values were derived from
22 experimental data using the Sigmoidal dose–response fitting of GraphPad Prism software. To
23 remove possible false positive results, for each compound concentration a blank analysis was
24 carried out, and the final absorbance results were obtained deducting the absorbance produced by
25 the presence of all the components except MAGL in the same conditions. In the enzyme kinetics
26 experiments, compound was tested in the presence of scalar concentrations of 4-NPA. It was added
27 in scalar amounts (concentration range = 1–10 μM) to a reaction mixture containing Tris buffer and
28 scalar concentrations of 4-NPA (15–1400 μM). Finally, MAGL solution was added (11 ng/well).
29 The MAGL activity was measured by recording the increase in 4-nitrophenol absorbance using the
30 Victor X3 Microplates Reader (PerkinElmer®). The experimental data were analyzed by non-linear
31 regression analysis with GraphPad Prism software, using a second order polynomial regression
32 analysis, and by applying the mixed-model inhibition fit.
33
34
35
36
37
38
39
40
41
42
43
44
45
46
47
48
49
50
51
52
53
54
55
56
57
58
59
60

1
2
3 **FAAH inhibition assay.** The IC₅₀ values for compounds were generated in 96-well microtiter
4 plates. The FAAH reaction was conducted at room temperature at a final volume of 200 μL in 125
5 mM Tris buffer, pH 9.0, containing 1 mM EDTA and in the presence of BSA 0.1 mg/ml. A total of
6 150 μL of AMC arachidonoylamide 13.3 μM (final concentration = 10 μM) was added to 10 μL of
7 DMSO containing the appropriate amount of compound. The reaction was initiated by the addition
8 of 40 μL of FAAH (0.9 μg/well) in such a way that the assay was linear over 30 min. The final
9 concentration of the analyzed compounds ranged for from 200 to 0.0128 μM. After the reaction had
10 proceeded for 30 min, fluorescence values were then measured by using a Victor X3 PerkinElmer
11 instrument at an excitation wavelength of 340 nm and an emission of 460 nm. Two reactions were
12 also run: one reaction containing no compounds and the second one containing neither inhibitor nor
13 enzyme. IC₅₀ values were derived from experimental data using the Sigmoidal dose–response
14 fitting of GraphPad Prism software. To remove possible false positive results, for each compound
15 concentration a blank analysis was carried out, and the final fluorescence results were obtained
16 deducting the fluorescence produced by the presence of all the components except FAAH in the
17 same conditions.
18
19
20
21
22
23
24
25
26
27
28
29
30
31
32
33
34
35

36 **Cell viability assay.** OVSAHO, OVCAR3, COV318, CAOV3 and MRC5 (from ATCC) were
37 maintained at 37 °C in a humidified atmosphere containing 5% CO₂ accordingly to the supplier.
38 Normal (1.5×10^4) and tumor (5×10^2) cells were plated in 96-well culture plates. The day after
39 seeding, vehicle or compounds were added at different concentrations to the medium. Compounds
40 were added to the cell culture at a concentration ranging from 200 to 0.02 μM. Cell viability was
41 measured after 96 h according to the supplier (Promega, G7571) with a Tecan F200 instrument.
42 IC₅₀ values were calculated from logistical dose response curves. Averages were obtained from
43 three independent experiments, and error bars are standard deviations (n = 3).
44
45
46
47
48
49
50
51
52
53

54 **Western blot analysis.** Cancer cells were pelleted and resuspended into RIPA buffer supplemented
55 3 with a protease inhibitor mixture (Complete-EDTA, Roche, Switzerland) for protein extraction.³⁷
56 Fifty μg of proteins were run in 8% denaturing polyacrylamide gel. After electrophoresis, the
57
58
59
60

1
2
3 proteins were transferred on nitrocellulose membrane (Whatman International Ltd, UK). The
4
5 membranes were blocked with 5% (w/v) skim milk in Tris-buffered saline Tween 20 solution (TBS-
6
7 T) and incubated overnight with primary antibodies (Vinculin (sc-7649), 1:1000 from Santa Cruz,
8
9 CA, US; MAGL (Ab24701) 1:1000 from Abcam, Cambridge, UK). After washing, membranes
10
11 were incubated for 1 h with secondary antibodies in 5% milk TBS-T at RT, developed with
12
13 enhanced chemiluminescence (ECL) solution and visualized with ChemiDoc Imager instrument
14
15 (Bio-Rad Laboratories, CA, US).³⁸
16
17
18
19

20 21 SUPPORTING INFORMATION

22 Clustering analysis, docking results of compound **17c** and **17a**, MD simulation analysis of **17b**, ¹H-
23
24 NMR spectra of compound **12c**, interference analysis for compound **17b**, effect of DTT on the **17b**
25
26 inhibition properties, cell growth inhibitory activities of compounds **17b**, **2** and **3**, IC₅₀ plot of
27
28 MAGL inhibition of compound **43**, analytical data on intermediate compounds, HPLC
29
30 chromatograms and NMR spectra of the final compounds. This material is available free of charge
31
32 via the Internet at <http://pubs.acs.org>.
33
34
35

36 37 CORRESPONDING AUTHOR INFORMATION

38 Corresponding author phone: +39 0502219595; e-mail: tiziano.tuccinardi@unipi.it
39
40
41

42 43 ACKNOWLEDGMENTS

44
45 This work was supported by the University of Pisa under the PRA program (project PRA_2016_27
46
47 and PRA_2016_59).
48
49
50

51 52 ABBREVIATIONS USED

53
54 MAGL, monoacylglycerol lipase; AEA, anandamide; 2-AG, 2-arachidonoylglycerol; EAE,
55
56 experimental allergic encephalomyelitis; FAAH, fatty acid amide hydrolase; PAINS, pan assay
57
58 interference compounds; 4-NPA, 4-nitrophenylacetate; 4-NP, 4-nitrophenol; CG, conjugate
59
60

1
2
3 gradient; PME, Particle Mesh Ewald; GAFF, general Amber force field; ECL, enhanced
4
5 chemiluminescence.
6
7
8

9 10 REFERENCES

- 11 1. Pacher, P.; Batkai, S.; Kunos, G. The endocannabinoid system as an emerging target of
12 pharmacotherapy. *Pharmacol. Rev.* **2006**, *58*, 389-462.
13
- 14 2. Di Marzo, V. The endocannabinoid system: its general strategy of action, tools for its
15 pharmacological manipulation and potential therapeutic exploitation. *Pharmacol. Res.* **2009**, *60*, 77-
16 84.
17
- 18 3. Di Iorio, G.; Lupi, M.; Sarchione, F.; Matarazzo, I.; Santacroce, R.; Petruccelli, F.;
19 Martinotti, G.; Di Giannantonio, M. The endocannabinoid system: a putative role in
20 neurodegenerative diseases. *Int. J. High Risk Behav. Addict.* **2013**, *2*, 100-106.
21
- 22 4. Scalvini, L.; Piomelli, D.; Mor, M. Monoglyceride lipase: structure and inhibitors. *Chem.*
23 *Phys. Lipids* **2016**, *197*, 13-24.
24
- 25 5. Muccioli, G. G.; Labar, G.; Lambert, D. M. CAY10499, a novel monoglyceride lipase
26 inhibitor evidenced by an expeditious MGL assay. *Chembiochem* **2008**, *9*, 2704-2710.
27
- 28 6. Zvonok, N.; Pandarinathan, L.; Williams, J.; Johnston, M.; Karageorgos, I.; Janero, D. R.;
29 Krishnan, S. C.; Makriyannis, A. Covalent inhibitors of human monoacylglycerol lipase: ligand-
30 assisted characterization of the catalytic site by mass spectrometry and mutational analysis. *Chem.*
31 *Biol.* **2008**, *15*, 854-862.
32
- 33 7. King, A. R.; Lodola, A.; Carmi, C.; Fu, J.; Mor, M.; Piomelli, D. A critical cysteine residue
34 in monoacylglycerol lipase is targeted by a new class of isothiazolinone-based enzyme inhibitors.
35 *Br. J. Pharmacol.* **2009**, *157*, 974-983.
36
- 37 8. Long, J. Z.; Li, W.; Booker, L.; Burston, J. J.; Kinsey, S. G.; Schlosburg, J. E.; Pavon, F. J.;
38 Serrano, A. M.; Selley, D. E.; Parsons, L. H.; Lichtman, A. H.; Cravatt, B. F. Selective blockade of
39
40
41
42
43
44
45
46
47
48
49
50
51
52
53
54
55
56
57
58
59
60

1
2
3 2-arachidonoylglycerol hydrolysis produces cannabinoid behavioral effects. *Nat. Chem. Biol.* **2009**,
4
5 5, 37-44.

7 9. Matuszak, N.; Muccioli, G. G.; Labar, G.; Lambert, D. M. Synthesis and in vitro evaluation
8
9 of N-substituted maleimide derivatives as selective monoglyceride lipase inhibitors. *J. Med. Chem.*
10
11 **2009**, 52, 7410-7420.

13 10. Kapanda, C. N.; Masquelier, J.; Labar, G.; Muccioli, G. G.; Poupaert, J. H.; Lambert, D. M.
14
15 Synthesis and pharmacological evaluation of 2,4-dinitroaryldithiocarbamate derivatives as novel
16
17 monoacylglycerol lipase inhibitors. *J. Med. Chem.* **2012**, 55, 5774-5783.

18 11. Labar, G.; Wouters, J.; Lambert, D. M. A review on the monoacylglycerol lipase: at the
19
20 interface between fat and endocannabinoid signalling. *Curr. Med. Chem.* **2010**, 17, 2588-2607.

21 12. Schlosburg, J. E.; Blankman, J. L.; Long, J. Z.; Nomura, D. K.; Pan, B.; Kinsey, S. G.;
22
23 Nguyen, P. T.; Ramesh, D.; Booker, L.; Burston, J. J.; Thomas, E. A.; Selley, D. E.; Sim-Selley, L.
24
25 J.; Liu, Q. S.; Lichtman, A. H.; Cravatt, B. F. Chronic monoacylglycerol lipase blockade causes
26
27 functional antagonism of the endocannabinoid system. *Nat. Neurosci.* **2010**, 13, 1113-1119.

28 13. King, A. R.; Dotsey, E. Y.; Lodola, A.; Jung, K. M.; Ghomian, A.; Qiu, Y.; Fu, J.; Mor, M.;
29
30 Piomelli, D. Discovery of potent and reversible monoacylglycerol lipase inhibitors. *Chem. Biol.*
31
32 **2009**, 16, 1045-1052.

33 14. Petronelli, A.; Pannitteri, G.; Testa, U. Triterpenoids as new promising anticancer drugs.
34
35 *Anticancer Drugs* **2009**, 20, 880-892.

36 15. Wang, L.; Wang, G.; Yang, D.; Guo, X.; Xu, Y.; Feng, B.; Kang, J. Euphol arrests breast
37
38 cancer cells at the G1 phase through the modulation of cyclin D1, p21 and p27 expression. *Mol.*
39
40 *Med. Rep.* **2013**, 8, 1279-1285.

41 16. Hernandez-Torres, G.; Cipriano, M.; Heden, E.; Bjorklund, E.; Canales, A.; Zian, D.; Feliu,
42
43 A.; Mecha, M.; Guaza, C.; Fowler, C. J.; Ortega-Gutierrez, S.; Lopez-Rodriguez, M. L. A reversible
44
45 and selective inhibitor of monoacylglycerol lipase ameliorates multiple sclerosis. *Angew. Chem.,*
46
47 *Int. Ed. Engl* **2014**, 53, 13765-13770.

- 1
2
3 17. Tuccinardi, T.; Granchi, C.; Rizzolio, F.; Caligiuri, I.; Battistello, V.; Toffoli, G.; Minutolo,
4 F.; Macchia, M.; Martinelli, A. Identification and characterization of a new reversible MAGL
5 inhibitor. *Bioorg. Med. Chem.* **2014**, *22*, 3285-3291.
6
7
8
9
10 18. Labar, G.; Bauvois, C.; Borel, F.; Ferrer, J. L.; Wouters, J.; Lambert, D. M. Crystal structure
11 of the human monoacylglycerol lipase, a key actor in endocannabinoid signaling. *ChemBiochem*
12 **2010**, *11*, 218-227.
13
14
15
16 19. Bertrand, T.; Auge, F.; Houtmann, J.; Rak, A.; Vallee, F.; Mikol, V.; Berne, P. F.; Michot,
17 N.; Cheuret, D.; Hoornaert, C.; Mathieu, M. Structural basis for human monoglyceride lipase
18 inhibition. *J. Mol. Biol.* **2010**, *396*, 663-673.
19
20
21
22
23 20. Schalk-Hihi, C.; Schubert, C.; Alexander, R.; Bayoumy, S.; Clemente, J. C.; Deckman, I.;
24 DesJarlais, R. L.; Dzordzorme, K. C.; Flores, C. M.; Grasberger, B.; Kranz, J. K.; Lewandowski, F.;
25 Liu, L.; Ma, H.; Maguire, D.; Macielag, M. J.; McDonnell, M. E.; Mezzasalma Haarlander, T.;
26 Miller, R.; Milligan, C.; Reynolds, C.; Kuo, L. C. Crystal structure of a soluble form of human
27 monoglyceride lipase in complex with an inhibitor at 1.35 Å resolution. *Protein Sci.* **2011**, *20*, 670-
28 683.
29
30
31
32
33
34
35
36 21. Griebel, G.; Pichat, P.; Beeske, S.; Leroy, T.; Redon, N.; Jacquet, A.; Francon, D.; Bert, L.;
37 Even, L.; Lopez-Grancha, M.; Tolstykh, T.; Sun, F.; Yu, Q.; Brittain, S.; Arlt, H.; He, T.; Zhang,
38 B.; Wiederschain, D.; Bertrand, T.; Houtmann, J.; Rak, A.; Vallee, F.; Michot, N.; Auge, F.; Menet,
39 V.; Bergis, O. E.; George, P.; Avenet, P.; Mikol, V.; Didier, M.; Escoubet, J. Selective blockade of
40 the hydrolysis of the endocannabinoid 2-arachidonoylglycerol impairs learning and memory
41 performance while producing antinociceptive activity in rodents. *Sci. Rep.* **2015**, *5*, 7642.
42
43
44
45
46
47
48
49 22. Wang, X.; Sarris, K.; Kage, K.; Zhang, D.; Brown, S. P.; Kolasa, T.; Surowy, C.; El
50 Kouhen, O. F.; Muchmore, S. W.; Brioni, J. D.; Stewart, A. O. Synthesis and evaluation of
51 benzothiazole-based analogues as novel, potent, and selective fatty acid amide hydrolase inhibitors.
52 *J. Med. Chem.* **2009**, *52*, 170-180.
53
54
55
56
57
58
59
60

- 1
2
3 23. Nomura, D. K.; Long, J. Z.; Niessen, S.; Hoover, H. S.; Ng, S. W.; Cravatt, B. F.
4
5 Monoacylglycerol lipase regulates a fatty acid network that promotes cancer pathogenesis. *Cell*
6
7 **2010**, *140*, 49-61.
8
9
10 24. Baell, J. B.; Holloway, G. A. New substructure filters for removal of pan assay interference
11
12 compounds (PAINS) from screening libraries and for their exclusion in bioassays. *J. Med. Chem.*
13
14 **2010**, *53*, 2719-2740.
15
16 25. Shoichet, B. K. Screening in a spirit haunted world. *Drug Discovery Today* **2006**, *11*, 607-
17
18 615.
19
20 26. Dahlin, J. L.; Nissink, J. W.; Strasser, J. M.; Francis, S.; Higgins, L.; Zhou, H.; Zhang, Z.;
21
22 Walters, M. A. PAINS in the assay: chemical mechanisms of assay interference and promiscuous
23
24 enzymatic inhibition observed during a sulfhydryl-scavenging HTS. *J. Med. Chem.* **2015**, *58*, 2091-
25
26 2113.
27
28
29 27. Dahlin, J. L.; Walters, M. A. How to triage PAINS-full research. *Assay Drug Dev. Technol.*
30
31 **2016**, *14*, 168-174.
32
33 28. Del Carlo, S.; Manera, C.; Chicca, A.; Arena, C.; Bertini, S.; Burgalassi, S.; Tampucci, S.;
34
35 Gertsch, J.; Macchia, M.; Saccomanni, G. Development of an HPLC/UV assay for the evaluation of
36
37 inhibitors of human recombinant monoacylglycerol lipase. *J. Pharm. Biomed. Anal.* **2015**, *108*, 113-
38
39 121.
40
41
42 29. Berman, H. M.; Westbrook, J.; Feng, Z.; Gilliland, G.; Bhat, T. N.; Weissig, H.; Shindyalov,
43
44 I. N.; Bourne, P. E. The protein data bank. *Nucleic Acids Res.* **2000**, *28*, 235-242.
45
46
47 30. Case, D. A.; Berryman, J. T.; Betz, R. M.; Cerutti, D. S.; III, T. E. C.; Darden, T. A.; Duke,
48
49 R. E.; Giese, T. J.; Gohlke, H.; Goetz, A. W.; Homeyer, N.; Izadi, S.; Janowski, P.; Kaus, J.;
50
51 Kovalenko, A.; Lee, T. S.; LeGrand, S.; Li, P.; Luchko, T.; Luo, R.; Madej, B.; Merz, K. M.;
52
53 Monard, G.; Needham, P.; Nguyen, H.; Nguyen, H. T.; Omelyan, I.; Onufriev, A.; Roe, D. R.;
54
55 Roitberg, A.; Salomon-Ferrer, R.; Simmerling, C. L.; Smith, W.; Swails, J.; Walker, R. C.; Wang,
56
57
58
59
60

1
2
3 J.; Wolf, R. M.; Wu, X.; York, D. M.; Kollman, P. A. *AMBER*, version 14. University of California:
4
5 San Francisco, CA, 2015.

6
7 31. *Maestro*, version 9.0. Schrödinger Inc: Portland, OR, 2009.

8
9 32. *Macromodel*, version 9.7. Schrödinger Inc: Portland, OR, 2009.

10
11 33. Morris, G. M.; Goodsell, D. S.; Halliday, R. S.; Huey, R.; Hart, W. E.; Belew, R. K.; Olson,
12
13 A. J. Automated docking using a Lamarckian genetic algorithm and an empirical binding free energy
14
15 function. *J. Comput. Chem.* **1998**, *19*, 1639-1662.

16
17 34. Morris, G. M.; Huey, R.; Lindstrom, W.; Sanner, M. F.; Belew, R. K.; Goodsell, D. S.;
18
19 Olson, A. J. AutoDock4 and AutoDockTools4: automated docking with selective receptor
20
21 flexibility. *J. Comput. Chem.* **2009**, *30*, 2785-2791.

22
23 35. York, D. M.; Darden, T. A.; Pedersen, L. G. The effect of long-range electrostatic
24
25 interactions in simulations of macromolecular crystals - a comparison of the Ewald and truncated
26
27 list methods. *J. Chem. Phys.* **1993**, *99*, 8345-8348.

28
29 36. Roe, D. R.; Cheatham, T. E., 3rd. PTRAJ and CPPTRAJ: software for processing and
30
31 analysis of molecular dynamics trajectory data. *J. Chem. Theory Comput.* **2013**, *9*, 3084-3095.

32
33 37. Hadla, M.; Palazzolo, S.; Corona, G.; Caligiuri, I.; Canzonieri, V.; Toffoli, G.; Rizzolio, F.
34
35 Exosomes increase the therapeutic index of doxorubicin in breast and ovarian cancer mouse models.
36
37
38
39
40
41 *Nanomedicine* **2016**, *11*, 2431-2441.

42
43 38. Roberti, A.; Rizzolio, F.; Lucchetti, C.; de Leval, L.; Giordano, A. Ubiquitin-mediated
44
45 protein degradation and methylation-induced gene silencing cooperate in the inactivation of the
46
47 INK4/ARF locus in Burkitt lymphoma cell lines. *Cell Cycle* **2011**, *10*, 127-134.

1
2
3
4
5
6
7
8
9
10
11
12
13
14
15
16
17
18
19
20
21
22
23
24
25
26
27
28
29
30
31
32
33
34
35
36
37
38
39
40
41
42
43
44
45
46
47
48
49
50
51
52
53
54
55
56
57
58
59
60

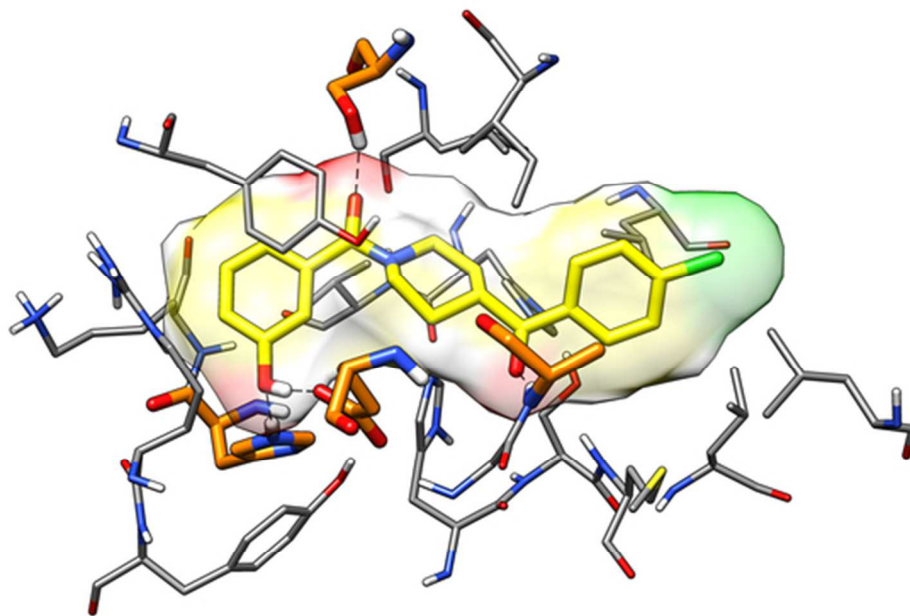


Table of Contents graphic

49x32mm (300 x 300 DPI)